IEEE Access
Multidisciplinary | Rapid Review | Open Access Journal

Received 7 March 2024, accepted 18 March 2024, date of publication 22 March 2024, date of current version 1 April 2024.

Digital Object Identifier 10.1109/ACCESS.2024.3380620

RESEARCH ARTICLE

Multi-Band Coupled-Fed Antenna for 4G LTE, Sub-6G, and WLAN Frequency Bands in Various Electronic Devices

MING-AN CHUNG, (Senior Member, IEEE), MING-CHANG LEE, CHIA-CHUN HSU, AND CHIA-WEI LIN

Department of Electronic Engineering, National Taipei University of Technology, Taipei City 10608, Taiwan

Corresponding author: Ming-An Chung (mingannchung@mail.ntut.edu.tw)

This work was supported by National Science and Technology Council, Taiwan, R.O.C. under Grant NSTC 112-2221-E-027-065-.

ABSTRACT This paper proposes a multi-band coupled-fed antenna (MBCFA) design for 4G LTE, Sub-6G, and WLAN frequencies, suitable for electronic devices with different sizes and fully metallic backplates. The MBCFA structure can be replicated on the fully metallic backplates of laptops, tablets, or smartphones to form a multi-input multi-output (MIMO) antenna system. Each MBCFA at different positions on laptops and tablets exhibits similar resonance characteristics, highlighting its high robustness and stability. The proposed MBCFA is manufactured using low-cost FR4 material. The overall size of MBCFA is 70 mm × 12.5 mm and an FR4 thickness of 0.8 mm, the measured reflection losses within the -6dB range are 740-990 MHz (250 MHz bandwidth), 1380-2640 MHz (1260 MHz bandwidth), and 4250-7330 MHz (3080 MHz bandwidth). The MBCFA's isolation levels in the 4G LTE frequency band are below −16 dB, while the remaining frequency bands have isolation levels below −20 dB. The maximum antenna gain is approximately 5 dBi, and the optimal antenna efficiency is 60%. The Equivalent Coupling Coefficient (ECC) for all frequency bands is below 0.5. Given the excellent antenna characteristics described above, the proposed multi-band coupled-fed antenna is an outstanding candidate for laptop, tablet, and smartphone antennas.

INDEX TERMS 4G LTE, ECC, MIMO, sub-6G, WLAN.

I. INTRODUCTION

The deployment of 5G telecommunication systems in electronic devices such as smartphones, laptops, and tablets has become increasingly prevalent, often in conjunction with the previous generation 4G LTE communication systems [1], [2], [3], [4], [5]. Typically, these devices employ separate antennas for 4G LTE and 5G systems [6], [7], allowing compact and slim designs that cater to specific frequency bands. However, the independent design of these antennas poses challenges in terms of spatial constraints and wavelength-related considerations, making it difficult to achieve optimal performance for both systems. Furthermore, the traditional placement of 4G LTE antennas on the sides of electronic devices has become increasingly challenging due to the decreasing height of the edge of the device caused by miniaturization [4], [8]. Some approaches integrate passive components, such as inductors or capacitors, with 4G LTE antennas on the device sides to achieve impedance matching and miniaturization [3], [4], [6], [9], [10]. However, this approach presents manufacturing issues, including component size, thickness, and process yield, leading to frequency deviations and requiring additional clearance areas to prevent short circuits.

In addition to 5G and 4G LTE systems, modern electronic devices often include wireless network communication systems such as WLAN or Bluetooth [3], [11], [12], [13], [14]. However, most antennas designed for 5G, 4G LTE and wireless network systems are independently developed [1], [2], [6], [14], [15], [16], [17], [18], [19], with only a few designs combining two of these systems [10]. There are also some studies that have only been designed for mobile phones

The associate editor coordinating the review of this manuscript and approving it for publication was Pavlos I. Lazaridis.

with respect to the LTE Band 42 (3.4-3.6 GHz), LTE Band 43 (3.6-3.8 GHz), or LTE Band 46 (5.15-5.925 GHz) in the context of Snb-6G [5], [8], [20]. Although the integration of sub-6G, 4G LTE, and WLAN bands into a multi-band single antenna design has been achieved [12], there is still a lack of LTE bands below 1GHz.

In many recent studies, in order to improve the communication performance of antennas, many researchers

have used multiple-input multiple-output (MIMO) antenna technology to improve communication capabilities in electronic products [2], [3], [5], [7], [9], [10], [13], [15], [17], [18], [21], [22], [23].

However, under the trend of miniaturization and thinner design of electronic products, when electronic products need to have antennas for 5G telecommunications systems, 4G LTE telecommunications systems, and WALN or Bluetooth antennas, this undoubtedly raises the threshold for antenna design.

Furthermore, the ground area of different sizes will also affect the results of the antenna design. Therefore, in electronic products or many research, the frequency bands of the aforementioned 5G telecommunications system, the frequency bands of the 4G LTE telecommunications system, and the frequency bands of WALN are designed as independent antenna structures [1], [2], [6], [14], [15], [16], [17], [18], [19], so that people have a variety of different antenna designs to meet the needs of use. For bands below 1GHz, the design often utilizes dipole antennas along with passive components to achieve the goal of antenna miniaturization. [1], [2], [17], [18]

Based on the factors mentioned above, this article designs a coupled antenna suitable for 5G, 4G LTE, WLAN, Bluetooth, and frequencies below 1GHz, without the use of passive components. The proposed antenna design is particularly suitable for metal backplanes found in popular

portable devices such as notebook computer screens, tablet computers, and mobile phones. When the seamless integration of multiple frequency bands on a single antenna is enabled, the requirements for antenna design in different frequency ranges are significantly reduced, eliminating the need for additional passive components to achieve matching conditions. As a result, the practicality of the proposed antenna is improved while also reducing manufacturing costs.

Furthermore, this paper investigates the performance of the Multiple-Input Multiple-Output (MIMO) technology when applied to diverse electronic products in a multi-path propagation environment. The study explores the suitability of the antenna to enhance communication quality and data transmission efficiency in real-world scenarios.

To ensure the safety of users, the paper also includes a simulation-based evaluation of the specific absorption rate (SAR) to assess any potential impact on the human body caused by the transmitting power of the antenna. This vital assessment guarantees compliance with safety standards and regulations, making the antenna design suitable for commercial deployment in various electronic devices.

The following section provides an overview of the antenna design and simulation results, including the antenna evolution, S-parameters, surface current analysis, and isolation. Section III analyzes and compares the simulated and measured performance of the antenna, including S parameters, radiation patterns, gain, and efficiency. Section IV discusses the envelope correlation coefficient (ECC) in relation to MIMO antenna technology. Section V discusses the impact of external factors on antenna performance, including hands, batteries, and LCD modules. Section VI examines the specific absorption rate (SAR) of the antenna. Section VII presents a comparative analysis between the proposed antenna and recent related antenna research. Finally, the conclusions are drawn in Section VIII.

II. ANTENNA DESIGN

In this paper, a multi-band coupled-fed antenna (MBCFA) design for 4G LTE, Sub-6G, and WLAN is proposed on a FR4 substrate. The substrate has a thickness of 0.8mm ($\varepsilon r = 4.4$, $\tan\delta = 0.02$) and an overall size of 70 mm × 12.5 mm × 0.8 mm. The same geometrically shaped multi-band coupled-fed antenna is used on different-sized full metal backplanes from notebook computers and tablet computers, forming a 10 × 10 MIMO antenna system.

Additionally, the same geometrically shaped multi-band coupled-fed antenna is used on a full-metal backplane of a smartphone, forming a 2 × 2 MIMO antenna system. The full-metal panel size of the notebook computer is 330 mm × 220 mm × 0.8 mm, equivalent to a 16 inch notebook computer. The geometric structure of the notebook computer's metal backplane and antenna system is shown in Figure 1. The full-metal panel size of the tablet computer is 260 mm × 200 mm × 0.8 mm, equivalent to a 10-inch tablet computer. The geometric structure of the metal backplane and antenna system of the tablet computer is shown in Figure 2. The size of the full-metal panel of the smartphone is 70 mm × 120 mm × 0.8 mm, equivalent to a 6-inch smartphone. The geometric structure of the smartphone's metal backplane and antenna system is illustrated in Figure 3.

A. ANTENNA EVOLUTION

The MIMO antenna system used for laptop computers, tablets, and smartphones adopts the same MBCFA architecture. As shown in Figure 4, we will explain the evolutionary process of the MBCFA specifically designed for laptop computers. The evolution process aims to enhance impedance matching, radiation efficiency, and bandwidth coverage across multiple frequency bands.

The reflection coefficients, as depicted in Figure 5, provide information on the antenna's impedance matching and the extent of signal reflections. When these coefficients are analyzed, the performance of the MBCFA can be evaluated and optimized. The proposed MBCFA design for notebook computers ensures compatibility with multi-band operation, including the 4G LTE, Sub-6G, and WLAN frequency bands.

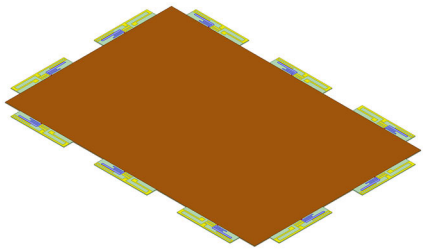

FIGURE 1. Geometric structure of the metal backplane and antenna system for notebook computers.

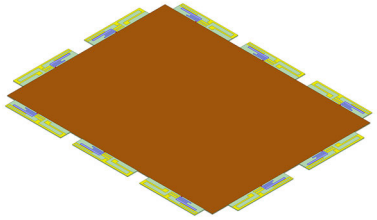

FIGURE 2. Geometric structure of the metal backplane and antenna system for tablet computers.

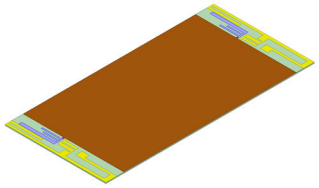

FIGURE 3. Geometric structure of the metal backplane and antenna system for smartphones.

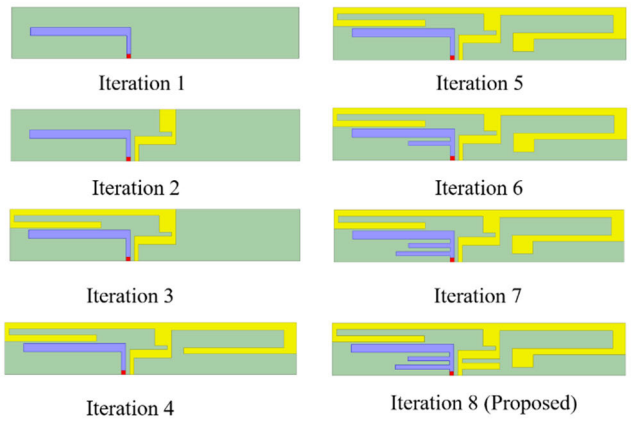

FIGURE 4. Evolution steps of the MBCFA for notebook computers.

By utilizing the MBCFA architecture, the MBCFA offers enhanced performance in terms of radiation patterns, gain, and efficiency.

The evolution steps of the MBCFA are depicted in Figure 4, while the reflection coefficients of the MBCFA are shown in Figure 5.

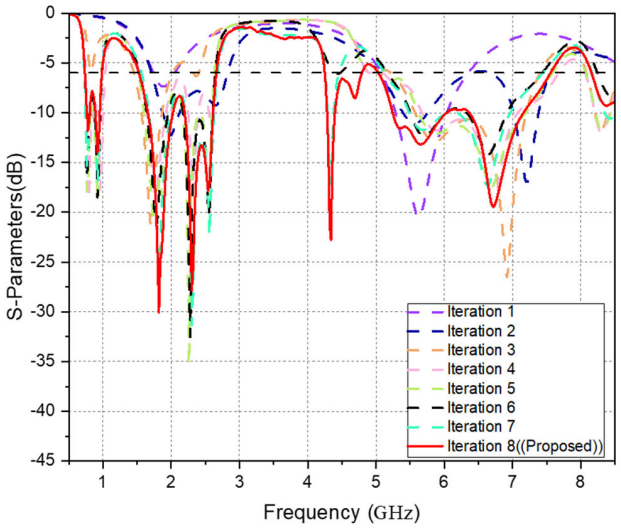

FIGURE 5. Reflection coefficients of the MBCFA for notebook computers.

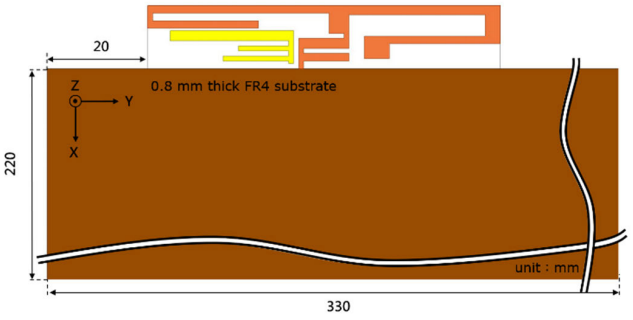

FIGURE 6. Schematic diagram of the MBCFA set on the full metal panel of the notebook computer.

As shown in Figure 6, during the iteration process, the full metal panel of the notebook computer is used as the ground plane for the antenna. The FR 4 substrate is placed at the top edge of the metal ground plane and is positioned 20mm away from the left edge of the metal ground plane. The FR 4 substrate is connected to one side of the full metal backplane, and the feeding point is designed at a position 28.5mm away from the left edge of the FR 4 substrate, followed by an L-shaped microstrip line that extends from the feeding point.

According to the previous literature, the design standard for the reflection coefficient of a 4G LTE antenna is below −6 dB [2], [3], [7]. Under this design standard, the MBCFA exhibits a resonance at 1.9GHz and 5.61GHz, respectively.

In iteration 2, an additional grounded microstrip line is added based on iteration 1, expanding the resonance frequencies of the antenna. Iteration 3 extends a microstrip line along the branch of iteration 2, generating a resonance at 0.8GHz, but the reflection coefficient does not meet the design standard.

In iteration 4, the antenna produces resonances at 0.74-1.03 GHz, 1.54-2.67 GHz, and 5.09-7.68 GHz within the resonance range of iteration 3.

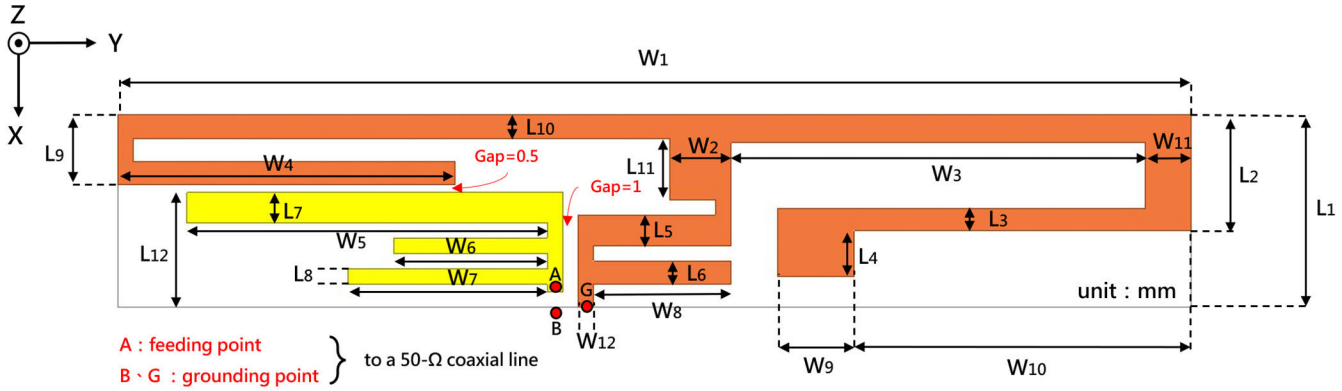

FIGURE 7. Recommended design dimensions of the proposed antenna.

TABLE 1. Antenna detailed dimensions Table.

Parameter	Value (mm)	Parameter	Value (mm)
L_1	12.5	W_1	70
L_2	7.5	W_2	4
L_3	0.5	W_3	27
L_4	3	W_4	22
L_5	2	W_5	23.5
L_6	1.5	W_6	10
L_7	2	W_7	13
L_8	1	W_8	9
L_9	1	W_9	5
L_{10}	4.5	W_{10}	22
L_{11}	1.5	W_{11}	3
L_{12}	4	W_{12}	1
L_{13}	7.5	W_{13}	1
L_{14}	1.8	*Gap2*	1
Gap1	0.5	*Gap3*	1

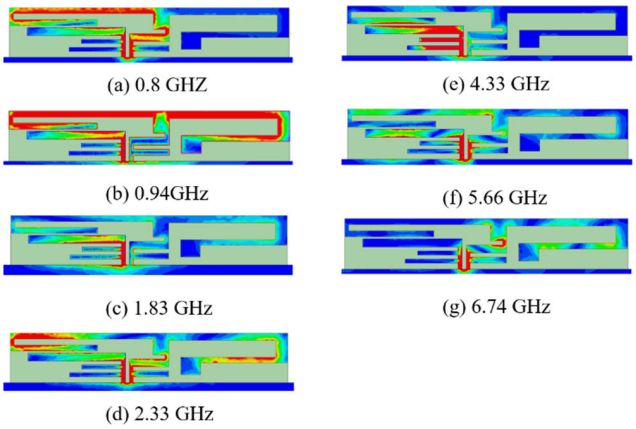

FIGURE 8. The current distributions of Ant. 1 in different frequency bands: (a) 0.8 GHz, (b) 0.94 GHz, (c) 1.83 GHz, (d) 2.33 GHz, (e) 4.33 GHz, (f) 5.66 GHz, and (g) 6.74 GHz.

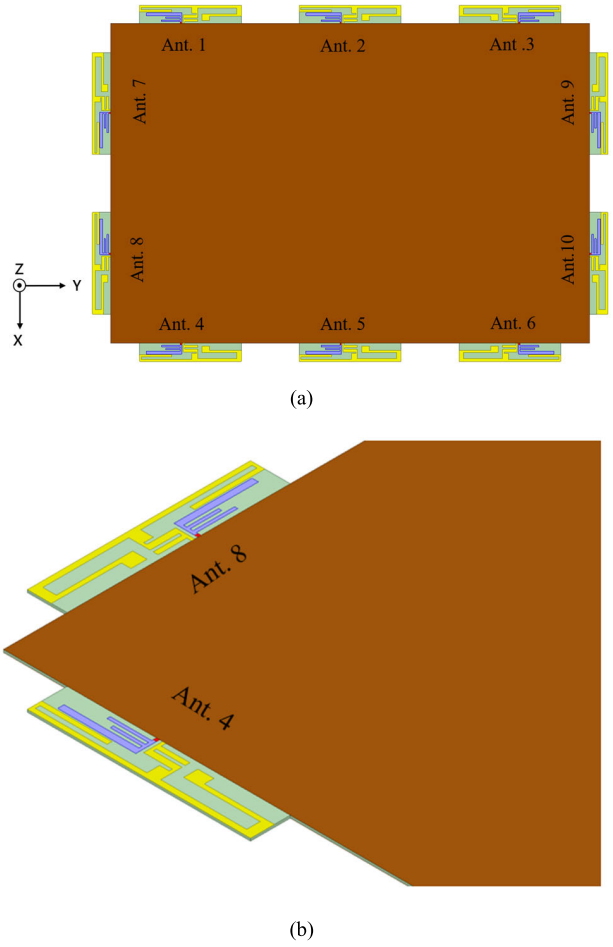

FIGURE 9. (a)Geometry of a 10 × 10 MIMO antenna system for a metal backplane of a notebook computer (b) Three-dimensional enlarged schematic diagram of Ant. 4 and Ant. 8.

Iterations 5-7 adjust the sub-6G resonance range while maintaining the resonances at 5.5 GHz and 7.2 GHz from iteration 4. By adding two microstrip lines between the iteration 1 antenna and the metal ground plane in iterations 5 and 6, the iteration 6 antenna exhibits resonances in various frequency bands while maintaining the resonances from iteration 4. In iteration 7, the resonance range of Sub-6G is adjusted to meet the design standard for the antenna's reflection coefficient. The proposed antenna extends the

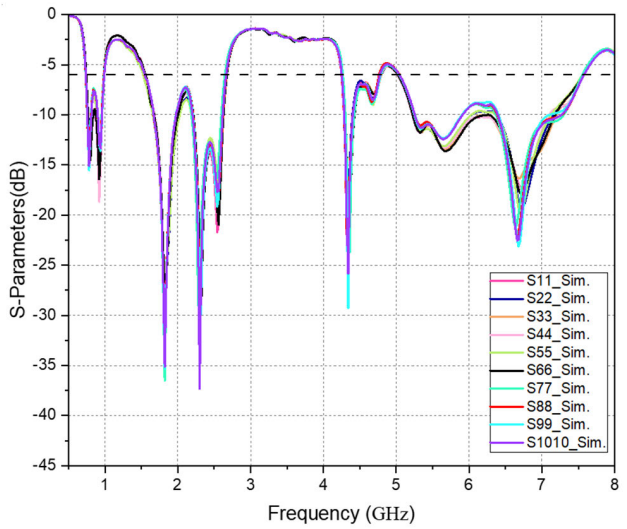

FIGURE 10. Results of the simulation of the reflection coefficient of a 10 × 10 MIMO antenna system with an all-metal backplane for a notebook computer.

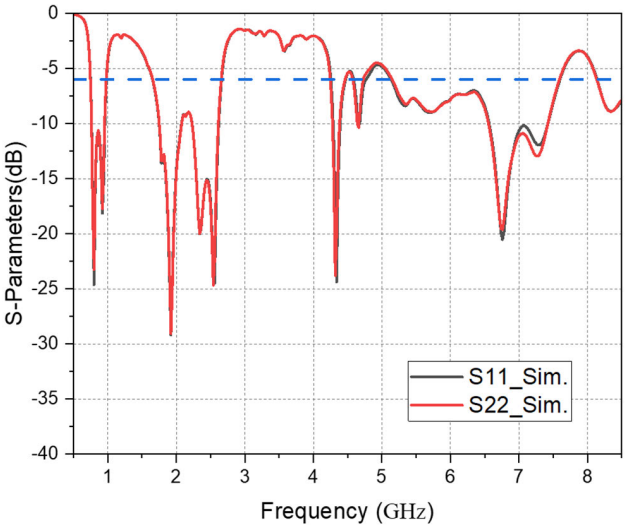

FIGURE 12. Simulation results of the reflection coefficient of a 10 × 10 MIMO antenna system for a smartphone with an all-metal backplane.

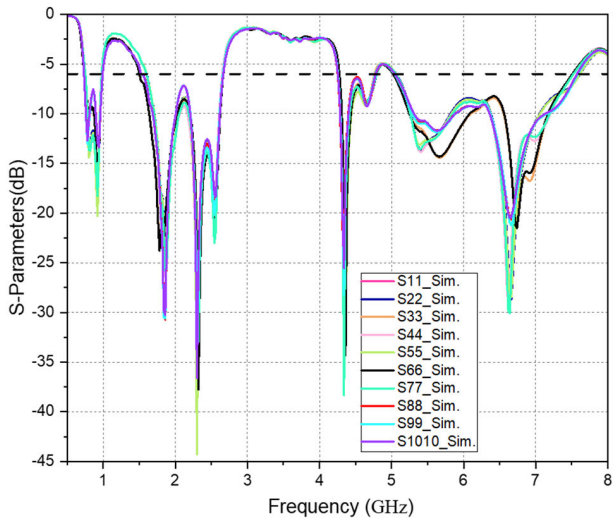

FIGURE 11. Simulation results of the reflection coefficient of a 10 × 10 MIMO antenna system with an all-metal backplane for a tablet PC.

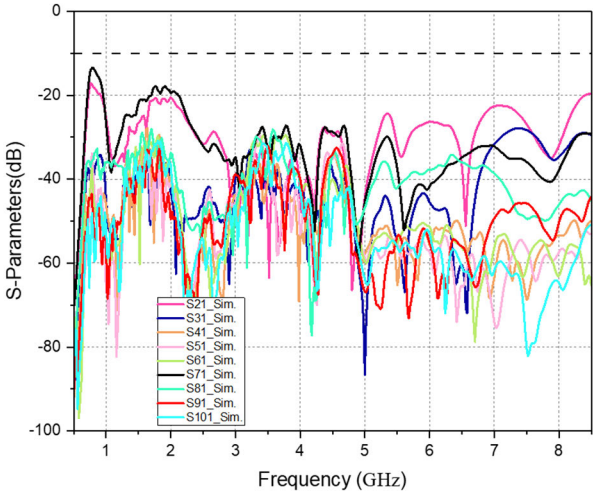

FIGURE 13. Simulation results of isolation S21~S101 of a 10 × 10 MIMO antenna system with a full metal backplane for a notebook computer.

resonance range of Sub-6G to 4.29-4.45GHz. Thus, under the design standard for the reflection coefficient, the proposed antenna in this study exhibits resonance frequencies of 0.74-0.98 GHz, 1.56-2.68 GHz, 4.29-4.45 GHz, and 5.02-7.57 GHz.

B. DESIGN DIMENSIONS OF THE PROPOSED ANTENNA

Based on the previous evolution of the antenna, the final dimensions of the proposed design evolved from the antenna are shown in Figure 7.

Furthermore, the detailed dimensions corresponding to the size codes in Figure 7 can be referenced in Table 1. Table 1 provides a comprehensive overview of the specific dimensions associated with each size code. Additionally, the overall dimensions of the substrate are 70 mm × 12.5 mm × 0.8 mm, which, based on the lowest frequency of 0.74 GHz in free space, calculates to an overall size of 0.17 λ × 0.03 λ × 0.00197 λ.

C. SURFACE CURRENT DISTRIBUTION OF THE PROPOSED ANTENNA

The antenna operates based on the flow of current entering from the feeding point and existing throughout the proposed antenna structure. When the antenna operates at the desired frequency, the current reaches its maximum amplitude, allowing electromagnetic waves to radiate from the antenna.

From Figure 8, it can be observed that at a frequency of 0.8 GHz, the current mainly flows around L_{12}, W_1, W_2, W_{12}, W_{13}, and W_{14}. At a frequency of 0.9 GHz, the

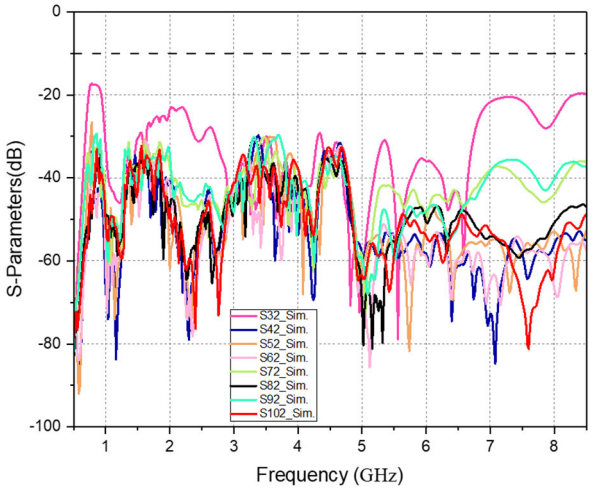

FIGURE 14. Simulation results of isolation S32∼S102 of a 10 × 10 MIMO antenna system with a full metal backplane for a notebook computer.

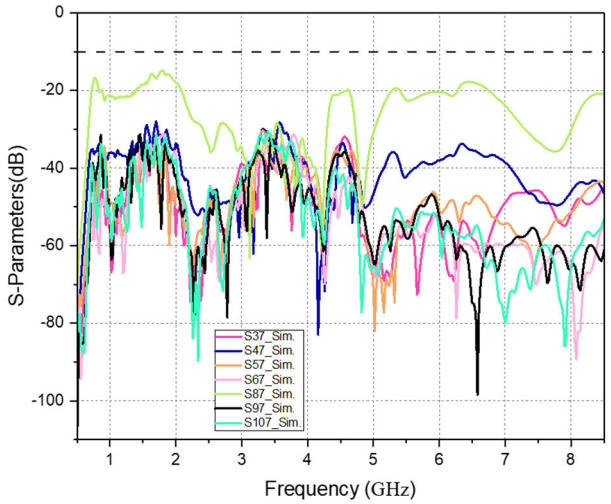

FIGURE 15. Results of the simulation of the isolation S37∼S107 of the 10 × 10 MIMO antenna system with the all-metal backplane of the notebook computer.

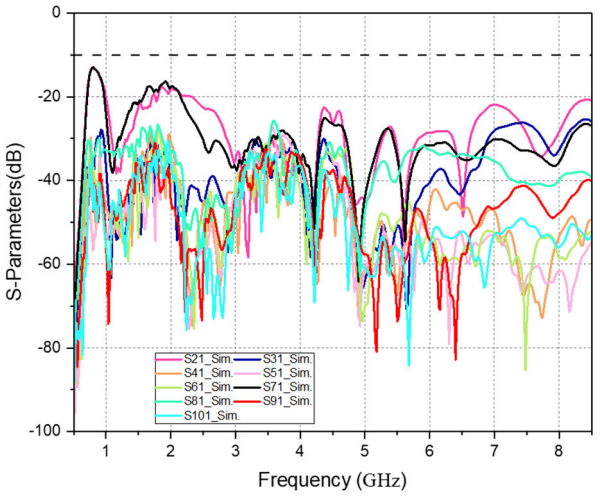

FIGURE 16. The simulation results of the isolation S21∼S101 of the 10 × 10 MIMO antenna system with the all-metal backplane of the Tablet.

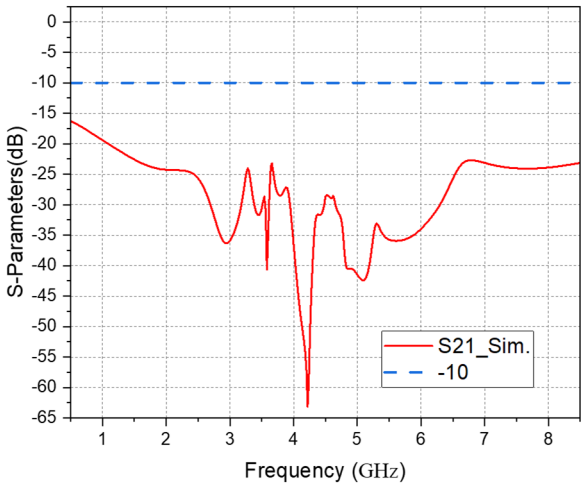

FIGURE 17. Simulation results of isolation S21 for a 2 × 2 MIMO antenna system with an all-metal backplane for a smartphone.

surface current flows between W_{13}, L_7, W_4, W_{14}, L_{11}, L_{12}, W_{11}, and L_3, coupling to generate the frequency range of 0.74-0.98 GHz. Similarly, the current flows between W_{13} and L_7 as well as between L_7, L_{11}, W_{12}, W_{13}, and W_{14}, coupling to generate the frequency range of 1.56-2.68 GHz. Additionally, the current flows between W_{13} and L_7 as well as between L_7 and L_9, coupling to generate the frequency range of 4.29-4.45 GHz. Furthermore, the current flows between W_{12} and W_{13}, producing the frequency range of 5.02-7.57 GHz. These observations correspond to the resonance frequencies generated during the antenna evolution analysis.

D. MIMO ANTENNA SYSTEM STRUCTURE

The proposed antennas were placed on the metal backplate of a notebook computer, which corresponds to a screen size equivalent to 16 inches. The geometric structure of the 10 × 10 MIMO antenna system on the metal backplate is shown in Figure 9. Ant. 1, as mentioned above, was placed at the top edge of the metal backplate, 20 mm away from the left edge. Ant. 2 was placed at the top edge of the metal backplate, with a distance of 40 mm from Ant. 1. Ant. 3 was the mirror image of Ant. 1, positioned on the metal backplate at a distance of 20 mm from the right edge and also 40 mm away from Ant. 2. Ant. 4, 5 and 6 were mirror images of Ant. 1, 2 and 3, placed at the bottom edge of the metal backplate. Ant. 7 was placed at the right edge of the metal backplate, with a distance of 20 mm from the top edge. Ant. 8 was placed at the right edge of the metal backplate, with a distance of 20 mm from the bottom edge. Ant. 9 and Ant.10 were mirror images of Ant. 7 and Ant.8, positioned at the bottom-left edge of the metal backplate.

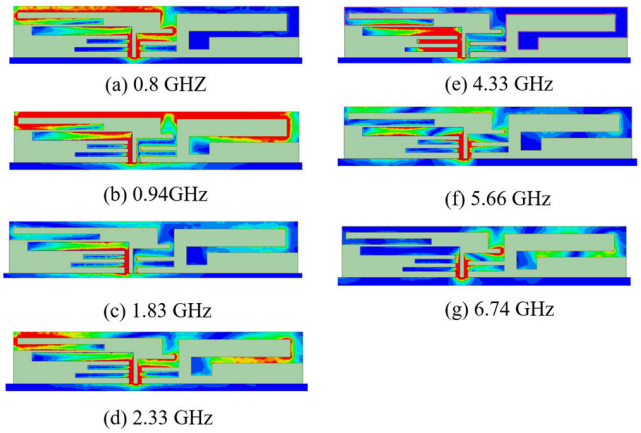

FIGURE 18. The current distributions of Ant. 2 in different frequency bands: (a) 0.8 GHz, (b) 0.94 GHz, (c) 1.83 GHz, (d) 2.33 GHz, (e) 4.33 GHz, (f) 5.66 GHz and (g) 6.74 GHz.

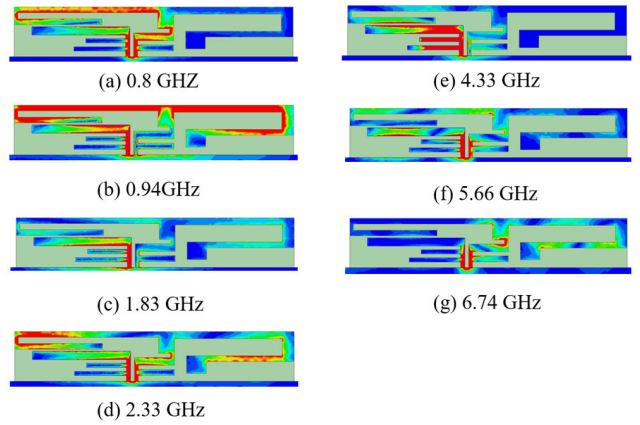

FIGURE 19. The current distributions of Ant. 7 in different frequency bands: (a) 0.8 GHz, (b) 0.94 GHz, (c) 1.83 GHz, (d) 2.33 GHz, (e) 4.33 GHz, (f) 5.66 GHz and (g) 6.74 GHz.

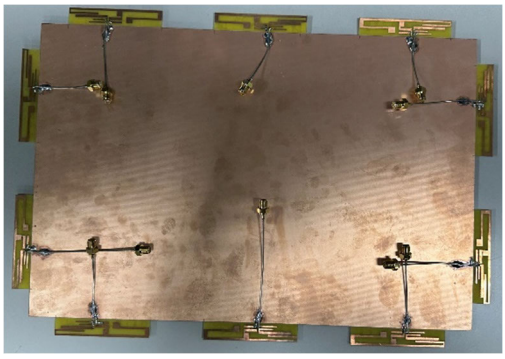

FIGURE 20. Photo of the 10 × 10 MIMO antenna system for the full metal backplane of the laptop.

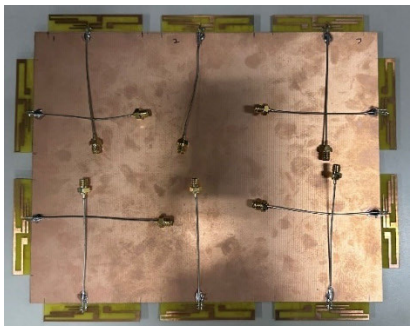

FIGURE 21. Photo of the 10 × 10 MIMO antenna system for the tablet's all-metal backplane.

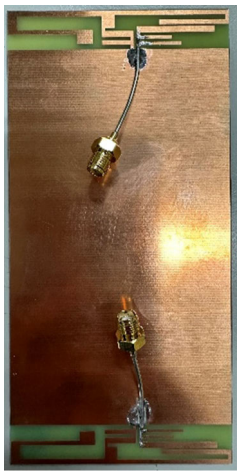

FIGURE 22. A photo of the 2 × 2 MIMO antenna system on the all-metal backplane of a smartphone.

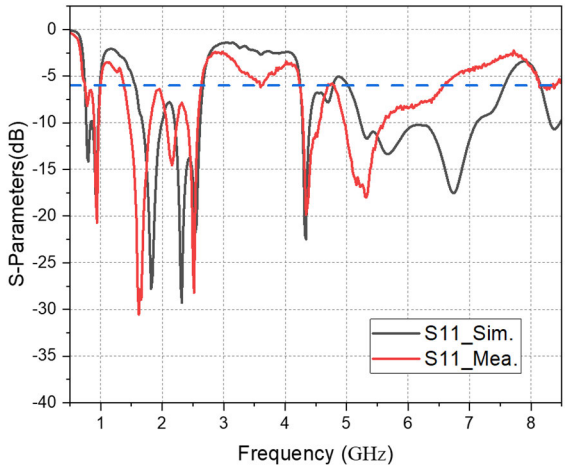

FIGURE 23. Simulated and Measured Reflection Coefficient of Ant. 1 for a 10 × 10 MIMO Antenna System with All-Metal Backplane for a Notebook Computer |S11|.

The simulated results of the 10 × 10 MIMO antenna system on the metal backplate of the notebook computer, using antenna simulation software as shown in Figure 10, the working frequency bands and resonance strengths were achieved that cover the operating frequency bands of 4G LTE, Sub-6G, and WLAN, while meeting the design criterion of reflection coefficient ≤ -6 dB. Furthermore, the working frequency bands and resonances of Ant. 1 to Ant.10 are nearly identical.

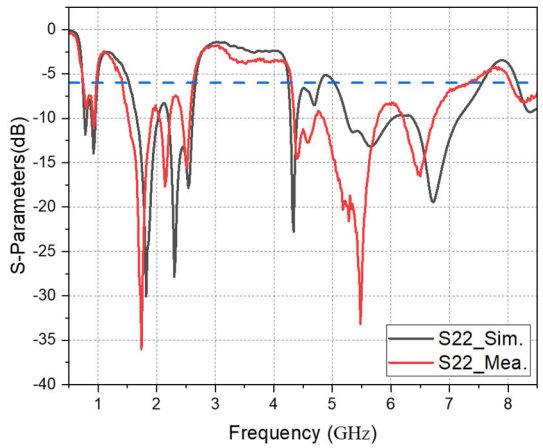

FIGURE 24. Simulated and Measured Reflection Coefficient of Ant. 2 for a 10 × 10 MIMO Antenna System with All-Metal Backplane for a Notebook Computer |S22|.

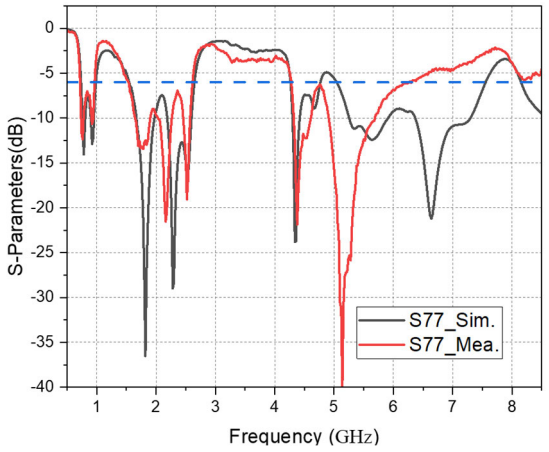

FIGURE 25. Simulation and measured reflection coefficients of Ant. 7 for a 10 × 10 MIMO antenna system with all metal backplane for Notebook Computers |S77|.

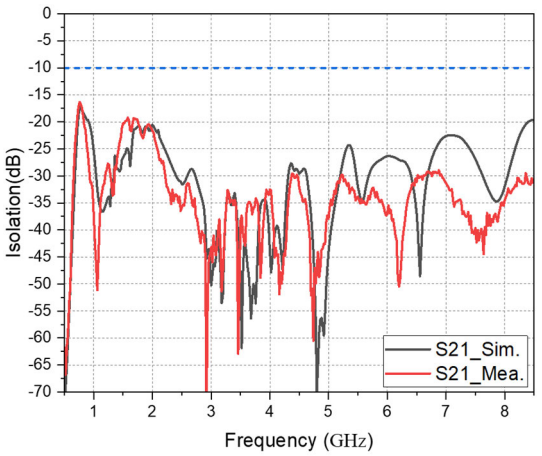

FIGURE 26. Simulation and Measured Isolation of Ant. 1 and Ant. 2 for a 10 × 10 MIMO Antenna System with All Metal Backplane for Notebook Computers |S21|.

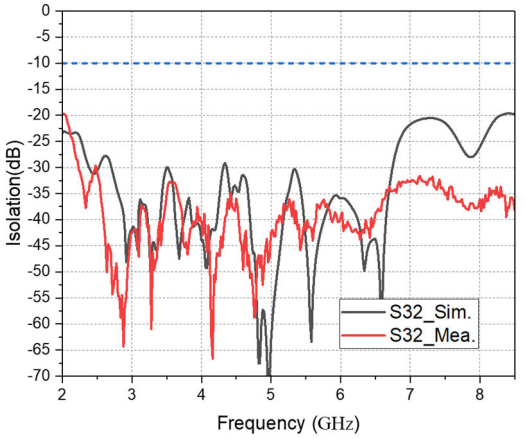

FIGURE 27. Simulation and Measured Isolation of Ant. 2 and Ant. 3 for a 10 × 10 MIMO Antenna System with All-Metal Backplane for Notebook Computer |S32|.

As shown in Figure 11, the simulated results of the 10 × 10 MIMO antenna system on the metal backplate of the tablet computer, using antenna simulation software, achieved working frequency bands and resonance strengths that cover the operating frequency bands of 4G LTE, Sub-6G and WLAN, while meeting the design criterion of reflection coefficient ≤ -6 dB. Additionally, the working frequency bands and resonances of Ant. 1 to 10 are nearly identical, and they are also different from the 10 × 10 MIMO antenna system on the metal backplate of the notebook computer.

Similarly, as shown in Figure 12, the simulated results of the 2 × 2 MIMO antenna system on the metal backplate of the smartphone, using antenna simulation software, achieved working frequency bands and resonance strengths that cover the operating frequency bands of 4G LTE, Sub-6G and WLAN, while meeting the design criterion of reflection coefficient ≤ -6 dB. The working frequency bands and resonances of Ant. 1 and Ant. 2 are nearly identical, and they are also similar to the 10 × 10 MIMO antenna system on the metal backplate of the notebook computer.

As shown in Figures 12 to 15, the simulated isolation of the 10 × 10 MIMO antenna system on the metal backplate of the notebook computer is below 20 dB, indicating good isolation between the MBCFAs. This is due to the placement of the antennas, with a minimum separation of at least 20 mm between the MBCFAs. However, for Ant. 1 and Ant. 2, as well as Ant. 1 and Ant. 7, which are placed within a separation of 20 mm, the simulated isolation is below 10 dB, but still within an acceptable range for reception.

It is essential to highlight that due to the mirror placement configuration of Ant. 1 to Ant. 3 and Ant. 4 to Ant. 6 in the 10 × 10 MIMO antenna system, as well as Ant. 7 to Ant. 8 and Ant. 9 to Ant. 10, and Ant. 1 and Ant. 3 being mirror placed,

Figures 13 to 15 illustrate the isolation of S21-S101, S32-S102, and S37-S107. These measurements represent the isolation among all antennas within the 10 × 10 MIMO antenna system.

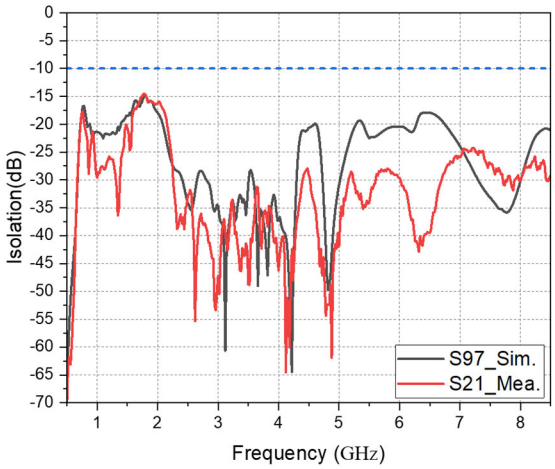

FIGURE 28. Simulation and measured isolation of Ant. 7 and Ant. 8 for a 10 × 10 MIMO antenna system with an all-metal backplane for a notebook |S87|.

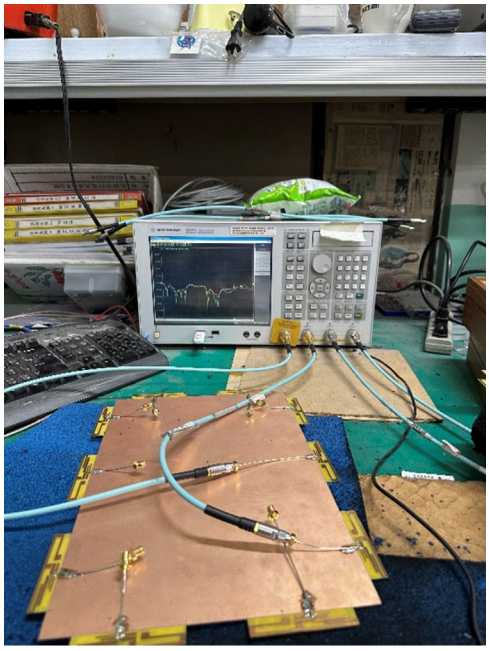

FIGURE 29. Schematic diagram of using a network analyzer to measure the 10 × 10 MIMO antenna system on the metal backplane of a laptop.

As shown in Figure 16, the simulated isolation of the 10 × 10 MIMO antenna system on the metal backplate of the tablet computer is below 20 dB, indicating good isolation between the antennas. The reason for this good isolation is that the antennas are placed at a minimum separation of at least 10 mm, with Ant. 1 and Ant. 2, as well as Ant. 1 and Ant. 7, placed within a separation of 10-20 mm. This results in simulated isolation below 10 dB, which is still within an acceptable reception range.

Furthermore, the simulated isolation of the 10 × 10 MIMO antenna system on the metal backplate of the tablet computer shows a trend similar to that of the 10 × 10 MIMO antenna system on the metal backplate of the notebook computer.

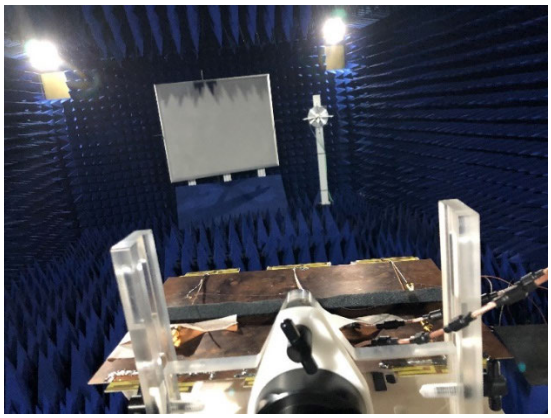

FIGURE 30. Photo of the installation of a 10 × 10 MIMO antenna system in the all-metal backplane of the notebook computer.

Therefore, the following implementation and measurement comparisons will focus on the 10 × 10 MIMO antenna system on the metal backplate of the notebook computer.

As shown in Figure 17, the simulated isolation of the 2 × 2 MIMO antenna system on the metal backplate of the smartphone is below 20 dB in the frequency range above 1 GHz, indicating good isolation between the antennas. However, the isolation below 1 GHz is lower than 15 dB. The reason for this lower isolation at lower frequencies is that the wavelength of the signals below 1 GHz is longer. When the antennas are positioned closer together, they are more prone to interference.

This issue of reduced isolation at lower frequencies is also observed in the 10 × 10 MIMO antenna systems on both the metal backplate of the notebook computer and the metal backplate of the tablet computer. This phenomenon highlights the challenges of achieving high isolation in compact devices where the antennas are in close proximity to each other at lower frequencies. Further optimization or isolation techniques may be required to improve the isolation in this frequency range.

Based on the description provided, it seems that the 10 × 10 MIMO antenna system in the metal backplate of the laptop exhibits symmetrical placement and mirror configurations for certain antennas. Specifically, Ant. 1, 2, and 7 represent similar configurations due to their symmetric and mirror positions. As a result, their geometrical shapes and current distributions are expected to be similar.

The simulation results shown in Figure 18 and Figure 19 also confirm this phenomenon, where the current distributions for Ant. 1, 2, and 7 are comparable. This similarity in current distributions is consistent with the symmetric and mirror placements of these antennas, as described in the laptop's 10 × 10 MIMO antenna system.

It is important to note that the placement of the proposed antennas in relation to the edges of the metal backplate significantly influences their performance. Specifically, if the antennas are positioned less than 20mm away from the edges, the isolation between Ant. 1 and Ant. 7 will exceed

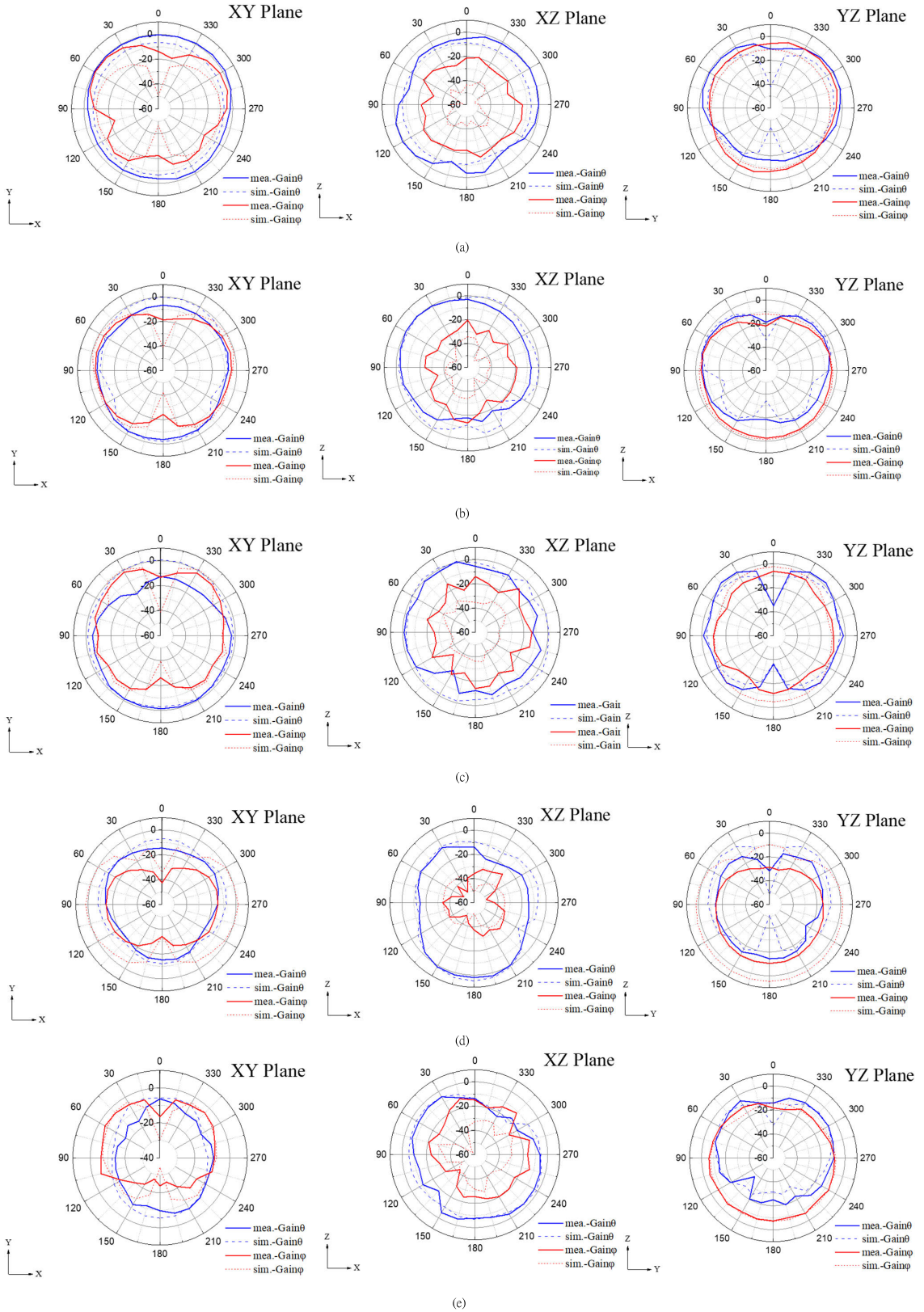

FIGURE 31. The 2D radiation pattern diagram of Ant. 1 of the 10 × 10 MIMO antenna system on the all-metal backplane of the notebook computer, (a) the 2D radiation pattern diagram of Ant. 1 at a frequency of 0.8 GHz, (b) 2D radiation pattern diagram of Ant. 1 at a frequency of 0.94 GHz, (c) 2D radiation pattern diagram of Ant. 1 at a frequency of 1.83 GHz, (d) 2D radiation pattern diagram of Ant. 1 at a frequency of 2.33 GHz, (e) 2D radiation pattern diagram of Ant. 1 at a frequency of 4.33 GHz.

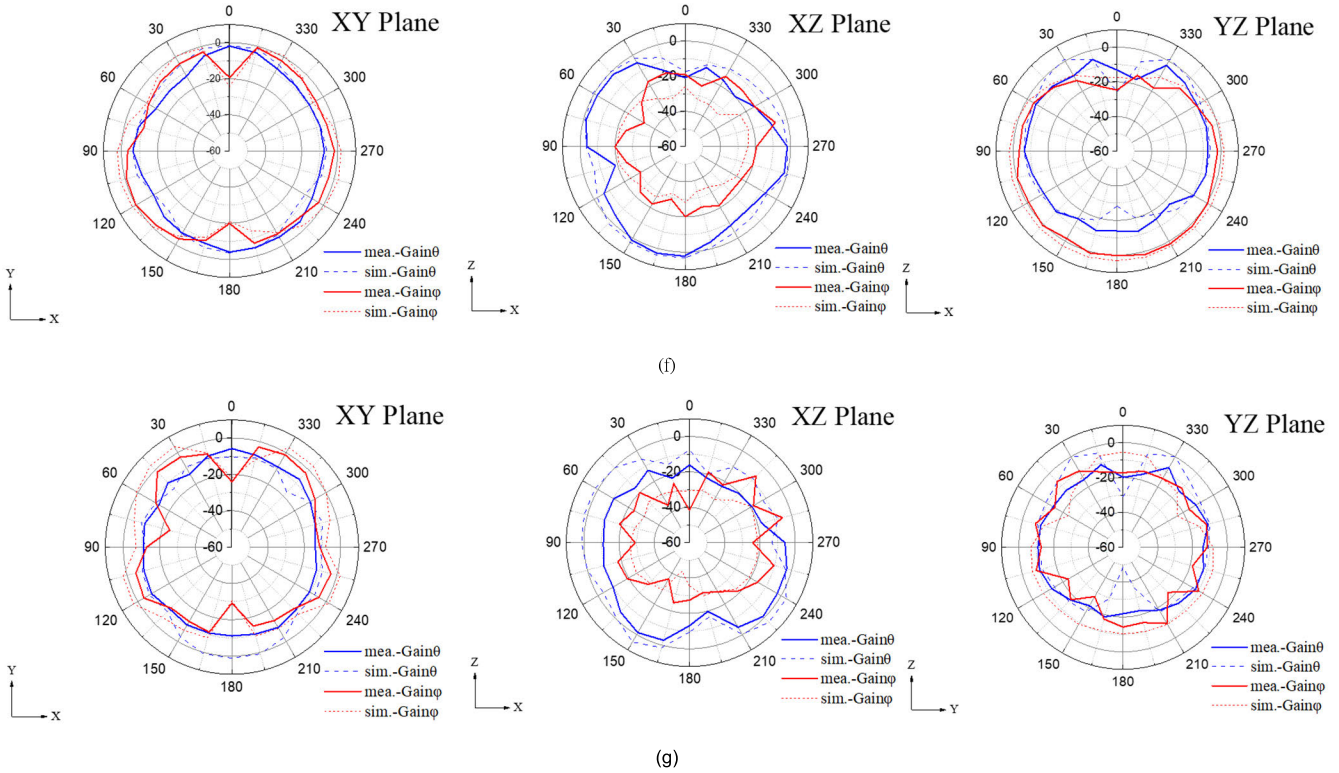

FIGURE 31. *(Continued.)* **The 2D radiation pattern diagram of Ant. 1 of the 10 × 10 MIMO antenna system on the all-metal backplane of the notebook computer, (f) 2D radiation pattern diagram of Ant. 1 at a frequency of 5.66 GHz, (g) 2D radiation pattern diagram of Ant. 1 1 at a frequency of 6.74 GHz.**

10dB. Therefore, in our proposed design, we have positioned the antennas at a distance of 20mm from the edges of the metal backplate and arranged all antennas symmetrically. Simulation results have demonstrated that all antennas exhibit similar characteristics, affirming the effectiveness of this strategic placement and symmetrical arrangement in ensuring optimal antenna performance.

Based on the information provided, it seems that the simulation results of the S-parameters for the 2 × 2 MIMO antenna system in the smartphone's full-metal backplate and the 10 × 10 MIMO antenna system in the tablet's full-metal backplate show similar trends compared to the 10 × 10 MIMO antenna system in the laptop's full-metal backplate.

In practical implementation and measurements, the comparison and analysis will be based on the laptop's MIMO antenna system using the 10 × 10 array on the full-metal backplate.

III. ANTENNA ANALYSIS

A. S-PARAMETERS

Figure 20 illustrates the physical configuration of the proposed 10 × 10 MIMO antenna system on the full-metal backplate of the laptop. Figure 21 illustrates the physical configuration of the proposed 10 × 10 MIMO antenna system on the full-metal backplate of the tablet. The MIMO antenna systems are implemented using FR-4 substrate material for the printed circuit board, while the full-metal backplate is made of two-sided copper metal. Each antenna is equipped with a 50 ohm feed connector and is positioned according to the placement in the simulation software. Ant. 1 to Ant. 10 are arranged around the perimeter of the full-copper metal surface.

Figure 22 shows the physical configuration of the proposed 2 × 2 MIMO antenna system on the full-metal backplate of the smartphone. The MIMO antenna system is implemented using FR-4 substrate material for the printed circuit board, while the full-metal backplate is made of two-sided copper metal. Each antenna is equipped with a 50 ohm feed connector and is positioned according to the placement in the simulation software. Ant. 1 to Ant. 2 are arranged on the upper and lower sides of the full-copper metal surface. As mentioned earlier, in the 10 × 10 MIMO antenna system on the full-metal backplate of a laptop or tablet, Ant. 1, 2, and 7 can represent their respective symmetric positions. Therefore, the following discussion will focus on Ant. 1, 3, and 7 for illustration.

As shown in Figure 23, Ant. 1 exhibits resonance frequencies at 0.8 GHz, 0.92 GHz, 1.82 GHz, 2.32 GHz, 2.54 GHz, 4.34 GHz, 4.7 GHz, 5.34 GHz, 5.68 GHz, and 6.8 GHz, as indicated by the reflection coefficient |S11|. The simulation results cover a frequency range of 0.74 GHz to 0.99 GHz (with a bandwidth of 250 MHz), 1.56 GHz

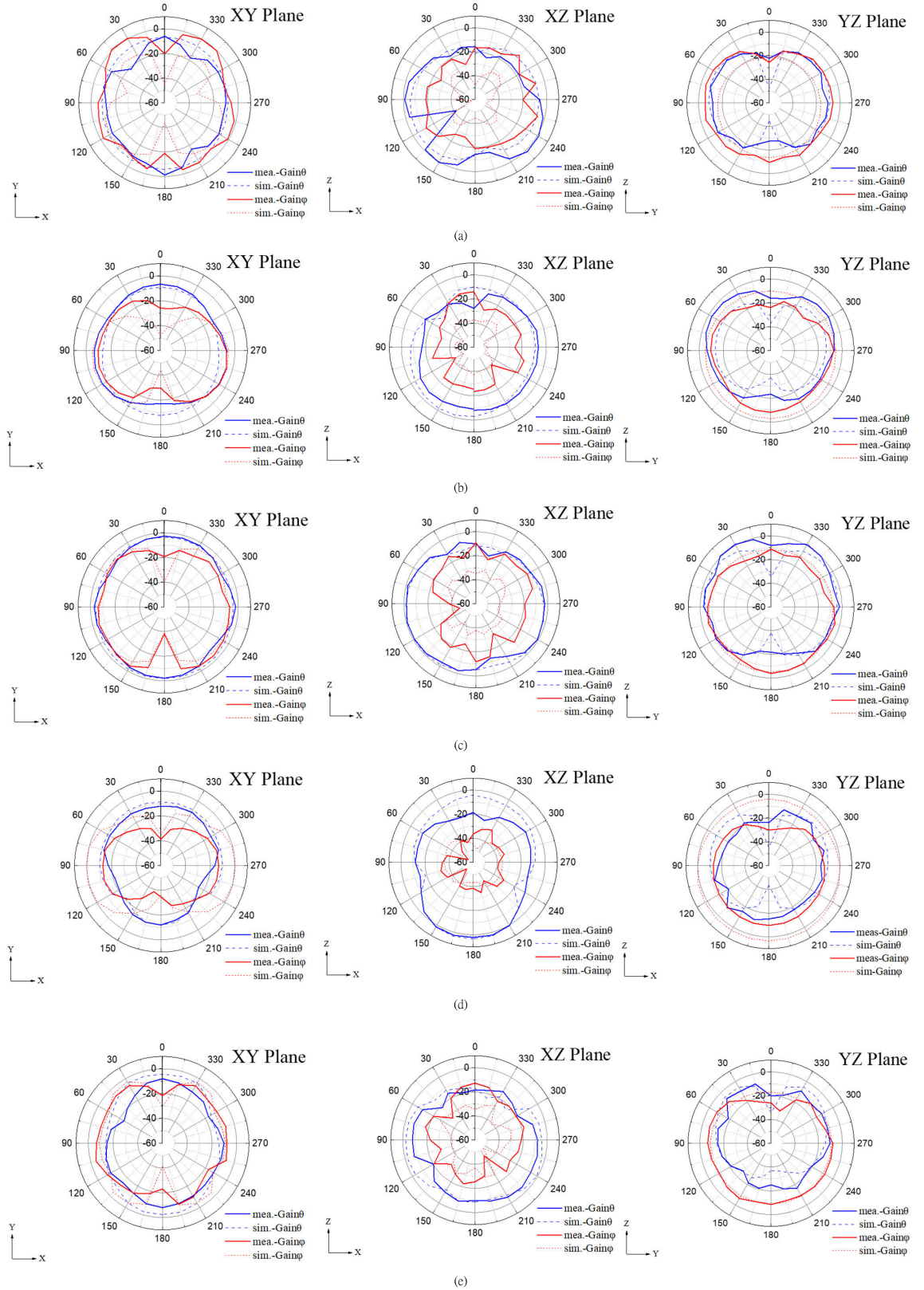

FIGURE 32. The 2D radiation pattern diagram of Ant. 2 of the 10 × 10 MIMO antenna system on the all-metal backplane of the notebook computer, (a) 2D radiation pattern diagram of Ant. 2 at a frequency of 0.8 GHz, (b) 2D radiation pattern diagram of Ant. 2 at a frequency of 0.94 GHz, (c) 2D radiation pattern diagram of Ant. 2 at a frequency of 1.83 GHz, (d) 2D radiation pattern diagram of Ant. 2 at a frequency of 2.33 GHz, (e) 2D radiation pattern diagram of Ant. 2 at 4.33 GHz.

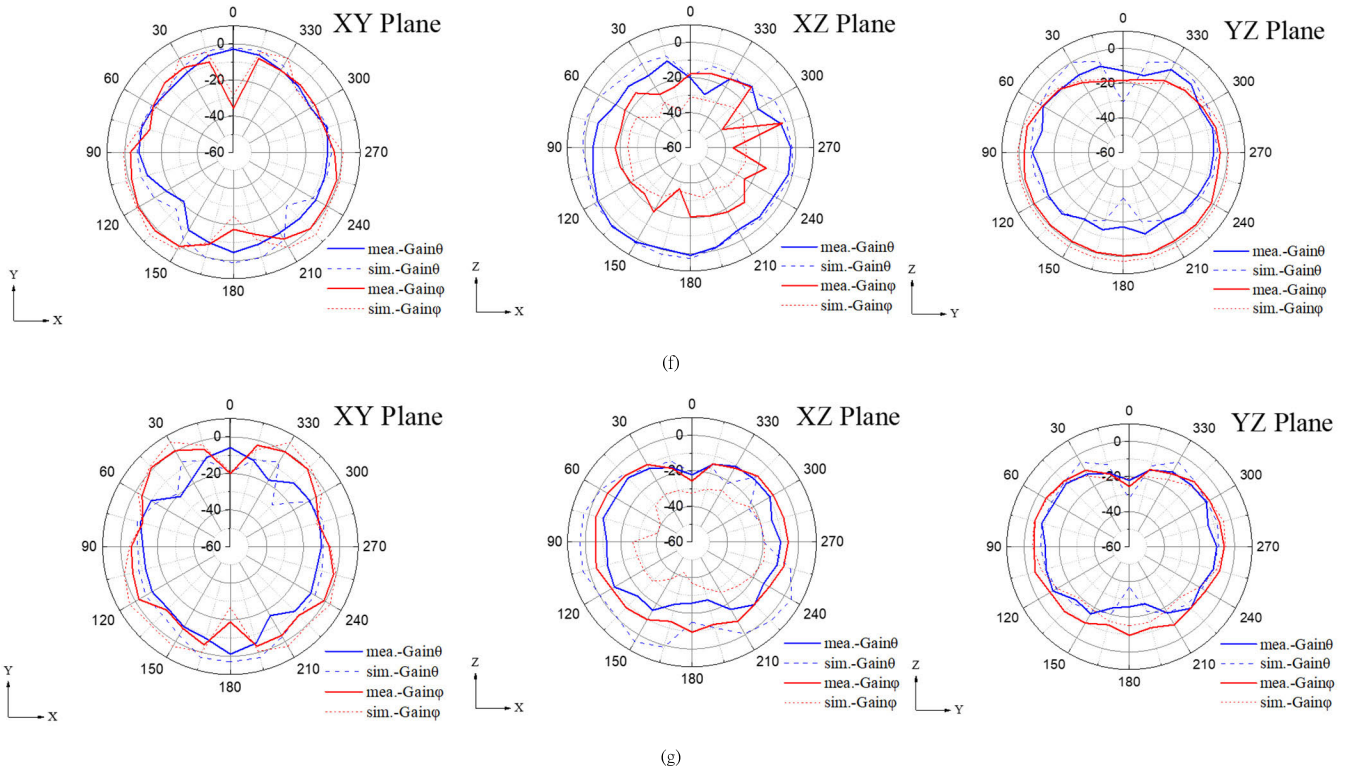

FIGURE 32. *(Continued.)* **The 2D radiation pattern diagram of Ant. 2 of the 10 × 10 MIMO antenna system on the all-metal backplane of the notebook computer, (f) 2D radiation pattern of Ant. 1 at 5.66 GHz, (g) 2D radiation pattern diagram of Ant. 2 at a frequency 6.74 GHz.**

to 2.66 GHz (with a bandwidth of 1.1 GHz), 4.25 GHz to 4.78 GHz (with a bandwidth of 0.53 GHz), and 5.02 GHz to 7.57 GHz (with a bandwidth of 2.55 GHz).

As shown in Figure 23, the measured reflection coefficient |S11| exhibits resonance frequencies at 0.78 GHz, 0.91 GHz, 1.63 GHz, 2.17 GHz, 2.5 GHz, 4.35 GHz, 4.53 GHz, 5.14 GHz, and 5.33 GHz. The measured results also cover a frequency range from 0.74 GHz to 1 GHz (with a bandwidth of 260 MHz), 1.38 GHz to 2.64 GHz (with a bandwidth of 1.24 GHz), 4.3 GHz to 4.7 GHz (with a bandwidth of 0.4 GHz), and 4.8 GHz to 6.58 GHz (with a bandwidth of 1.78 GHz), which is similar to the trend of simulated resonance frequencies.

As shown in Figure 24, the simulated reflection coefficient |S22| of Ant. 2 exhibits resonance frequencies at 0.8 GHz, 0.92 GHz, 1.82 GHz, 2.32 GHz, 2.54 GHz, 4.34 GHz, 4.7 GHz, 5.34 GHz, 5.68 GHz, and 6.8 GHz. The simulated results cover a frequency range from 0.74 GHz to 0.99 GHz (with a bandwidth of 250 MHz), 1.56 GHz to 2.66 GHz (with a bandwidth of 1.1 GHz), 4.25 GHz to 4.78 GHz (with a bandwidth of 0.53 GHz), and 5.02 GHz to 7.57 GHz(with a bandwidth of 2.55 GHz).

On the other hand, the measured reflection coefficient |S22| of Ant. 2 shows resonance frequencies at 0.78 GHz, 0.92 GHz, 1.73 GHz, 2.15 GHz, 2.52 GHz, 4.42 GHz, 4.6 GHz, 5.27 GHz, 5.49 GHz, and 6.46 GHz. The measured results cover a frequency range from 0.74 GHz to 0.97 GHz (with a bandwidth of 230 MHz), 1.41 GHz to 2.62 GHz (with a bandwidth of 1.21 GHz), and 4.3 GHz to 7.33 GHz (with a bandwidth of 3.03 GHz), which are in agreement with the simulated resonance frequency trend.

As shown in Figure 25, the simulated reflection coefficient |S77| for Ant. 7 exhibits resonance frequencies at 0.78 GHz, 0.92 GHz, 1.82 GHz, 2.29 GHz, 2.53 GHz, 4.35 GHz, 4.68 GHz, 5.33 GHz, 5.65 GHz, and 6.65 GHz. The simulated results cover a frequency range from 0.73 GHz to 0.99 GHz (with a bandwidth of 260 MHz), 1.55 GHz to 2.66 GHz (with a bandwidth of 1.11 GHz), 4.27 GHz to 4.77 GHz (with a bandwidth of 0.5 GHz), and 5.04 GHz to 7.56 GHz (with a bandwidth of 2.52 GHz).

On the other hand, the measured reflection coefficient |S77| shows resonance frequencies at 0.75 GHz, 0.93 GHz, 1.78 GHz, 2.17 GHz, 2.53 GHz, 4.38 GHz, 4.53 GHz, and 5.16 GHz. The measured results cover a frequency range from 0.72 GHz to 0.96 GHz (with a bandwidth of 240 MHz), 1.53 GHz to 2.61 GHz (with a bandwidth of 1.08 GHz), and 4.28 GHz to 6.3 GHz (with a bandwidth of 2.02 GHz). These measured resonance frequencies align well with the simulated trends.

In summary, the simulation and measurement results demonstrate similar resonance frequencies for Ant. 7, with the measured data closely match the simulated data in both frequency bands and bandwidths. The performance of the proposed MIMO antenna system for the metallic backplate of

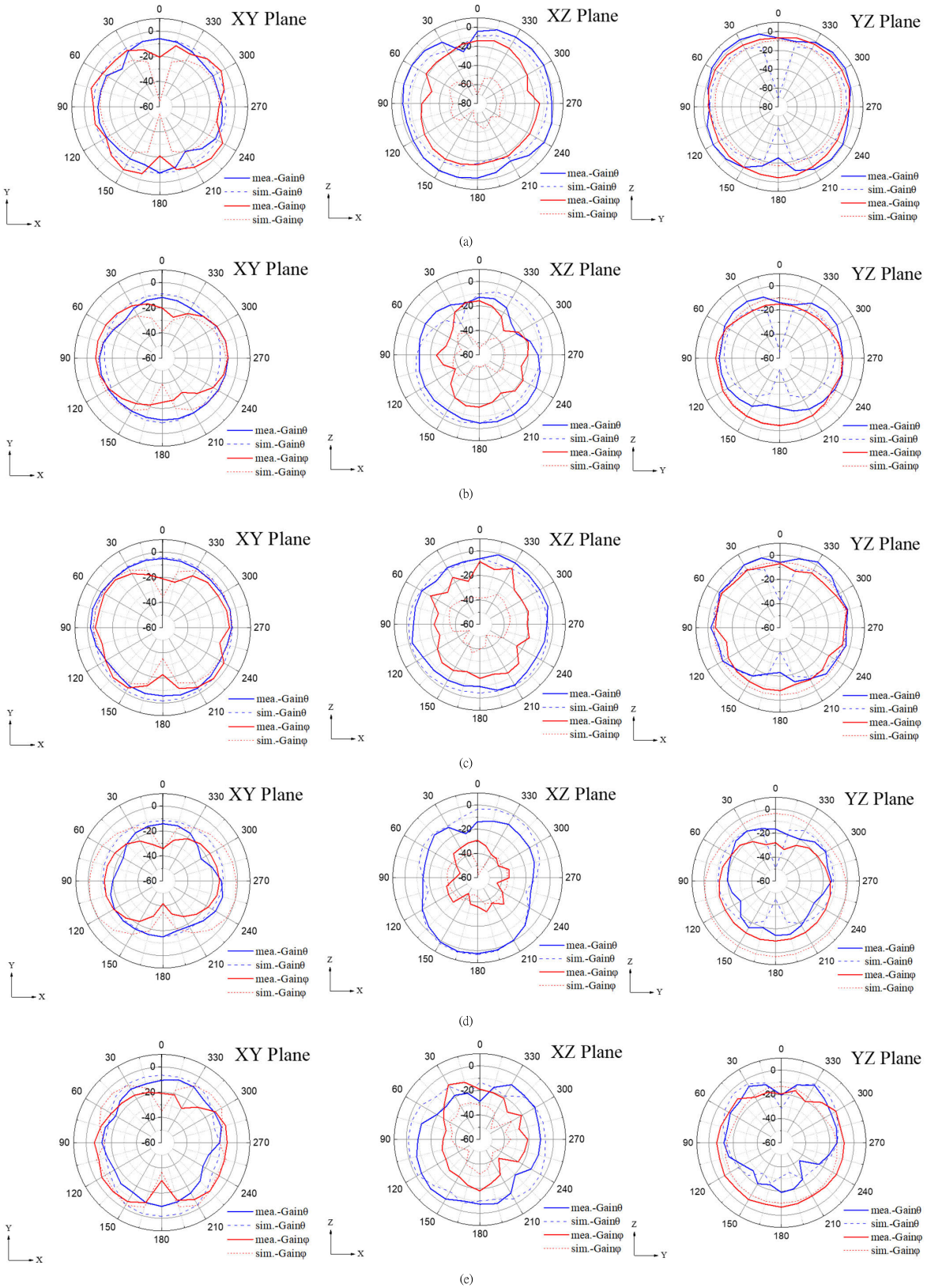

FIGURE 33. The 2D radiation pattern diagram of Ant. 7 of the 10 × 10 MIMO antenna system on the all-metal backplane of the notebook computer, (a) 2D radiation pattern diagram of Ant. 7 at a frequency of 0.8 GHz, (b) 2D radiation pattern diagram of Ant. 7 at a frequency of 0.94 GHz, (c) 2D radiation pattern diagram of Ant. 7 at a frequency of 1.83 GHz, (d) 2D radiation pattern diagram of Ant. 7 at a frequency of 2.33 GHz, (e) 2D radiation pattern diagram of Ant. 7 at a frequency of 4.33 GHz.

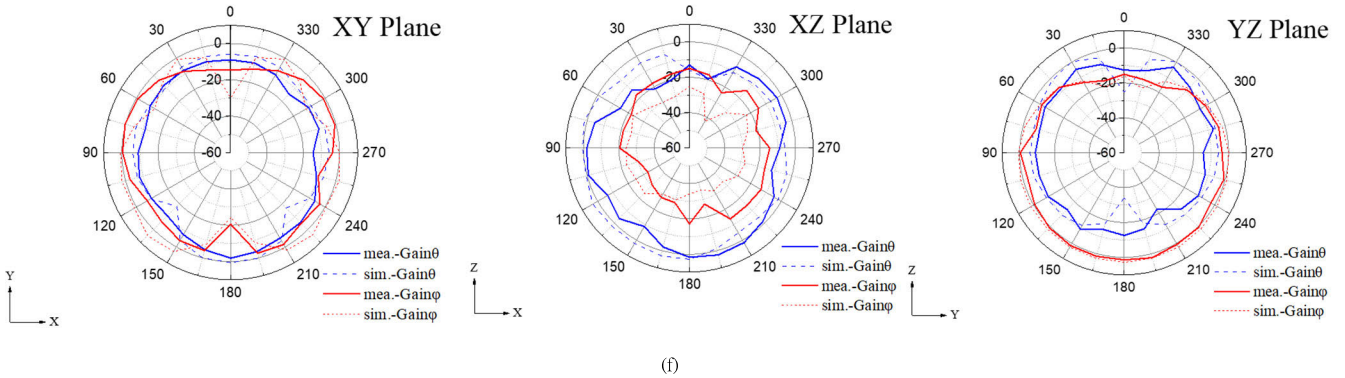

FIGURE 33. *(Continued.)*The 2D radiation pattern diagram of Ant. 7 of the 10 × 10 MIMO antenna system on the all-metal backplane of the notebook computer, (f) 2D radiation pattern diagram of Ant. 7 at a frequency of 5.66 GHz, (g) 2D radiation pattern diagram of Ant. 7 at a frequency of 6.74 GHz.

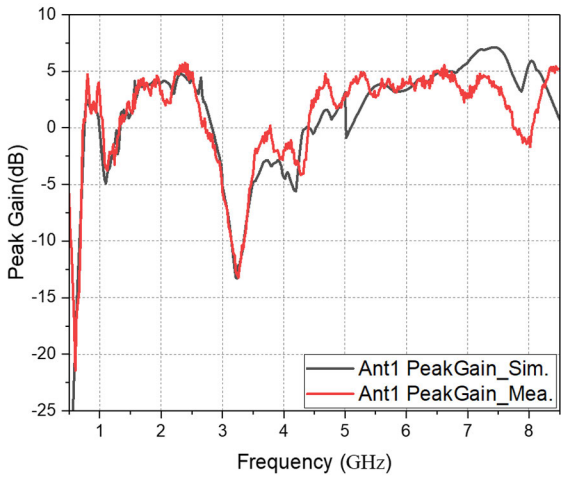

FIGURE 34. The simulated and measured gain values of Ant. 1 for a 10 × 10 MIMO antenna system with an all-metal backplane for a notebook computer.

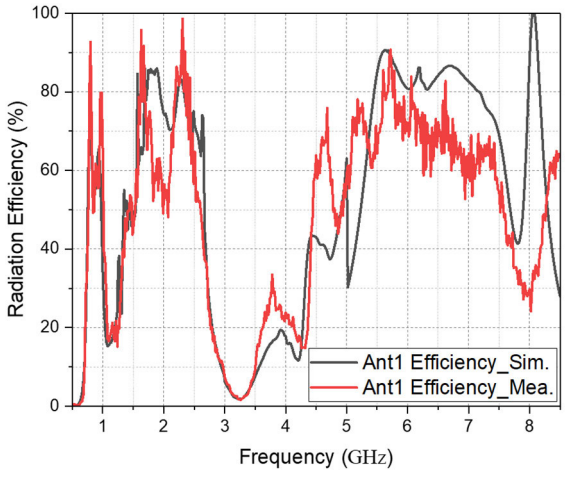

FIGURE 35. The simulated and measured efficiency values of Ant. 1 of a 10 × 10 MIMO antenna system with an all-metal backplane for a notebook computer.

a smart mobile phone is promising for 5G and other wireless communication applications.

As this study focusses on the 10 × 10 MIMO antenna system for both notebook and tablet computers, which involves ten antennas, the isolation between Ant. 1 to 10 is shown to be greater than 20 dB in the simulation results, indicating excellent isolation performance.

For clarity, we will now focus on describing the isolation between closely spaced antennas, namely, Ant. 1, 2, 7, and 8 in the 10 × 10 MIMO antenna system for the notebook computer.

In the simulation results, the isolation between Ant. 1 and 2 is also generally below 20 dB, which aligns with the measured isolation |S12|, as shown in Figure 26.

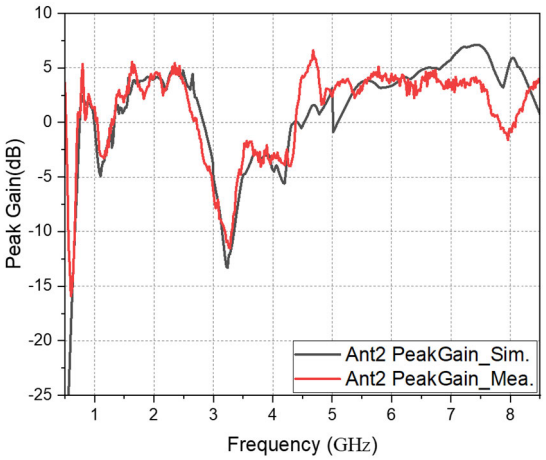

FIGURE 36. The simulated and measured gain values of Ant. 2 for a 10 × 10 MIMO antenna system with an all-metal backplane for a notebook computer.

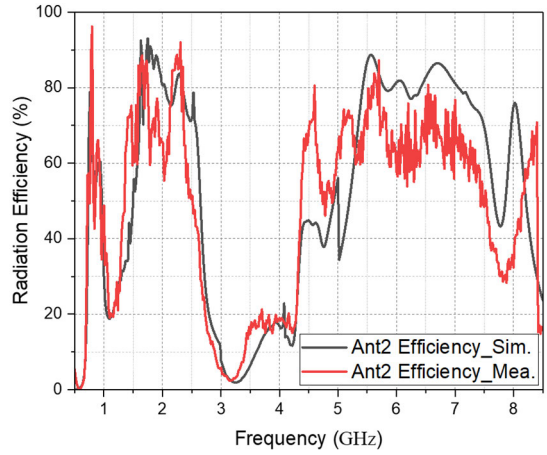

FIGURE 37. The simulated and measured efficiency values of Ant. 2 for a 10 × 10 MIMO antenna system with an all-metal backplane for a notebook computer.

In the simulation results, the isolation between Ant. 2 and 3 is also generally below 20 dB, which aligns with the measured isolation |S23|, as shown in Figure 27.

In the simulation results, the isolation between Ant. 7 and 8 is also generally below 20 dB, which aligns with the measured isolation |S78|, as shown in Figure 28.

As illustrated in Figure 29, the diagram shows the measurement of the reflection coefficient of the 10 × 10 MIMO antenna system, which is part of the metal backplate of the laptop proposed in this article, using an Agilent Technologies model E5071C network analyzer.

In conclusion, the simulation and measurement results of the reflection coefficients and isolation for Ant. 1, 2, and 7 agree well. The isolation between Ant. 1, 2, 7, and 8 is consistently below 10 dB, indicating that the 10 × 10 MIMO antenna system on the metal backplate of the notebook computer exhibits excellent isolation performance.

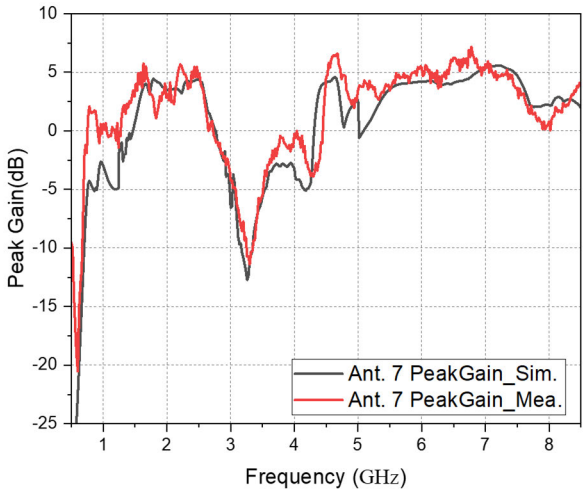

FIGURE 38. The simulated and measured gain values of Ant. 7 for a 10 × 10 MIMO antenna system with an all-metal backplane for a notebook computer.

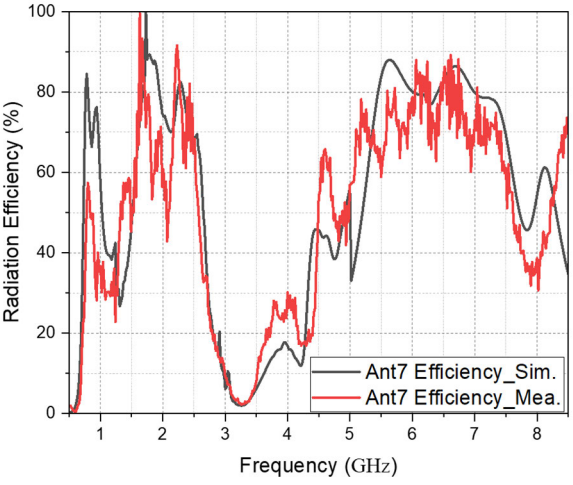

FIGURE 39. The simulated and measured efficiency values of Ant. 7 for a 10 × 10 MIMO antenna system with an all-metal backplane for a notebook computer.

B. FAR-FIELD RADIATION PATTERNS

Based on the simulation results in Figure 10, it is evident that the resonant modes of Ant. 1 to 10 are very similar. Therefore, for the subsequent far-field measurements, this study will focus on comparing the simulated and measured radiation patterns of Ant. 1, 2, and 7 as representatives of all the antennas.

The measurement setup utilized in this study is a standard far-field anechoic chamber. The network analyzer used is the Anritsu MS46524B model. The horn antenna used for measurements in the chamber operates in the frequency range of 0.1 to 8 GHz.

In Figure 30, a photo of the 10 × 10 MIMO antenna system with a metal backplate for a laptop, taken within the far-field anechoic chamber. The setup of this system

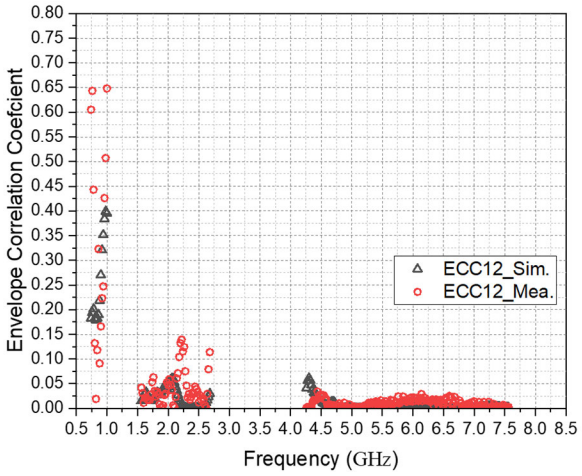

FIGURE 40. Comparison diagram of ECC simulation and actual measurement of Ant. 1 and Ant. 2.

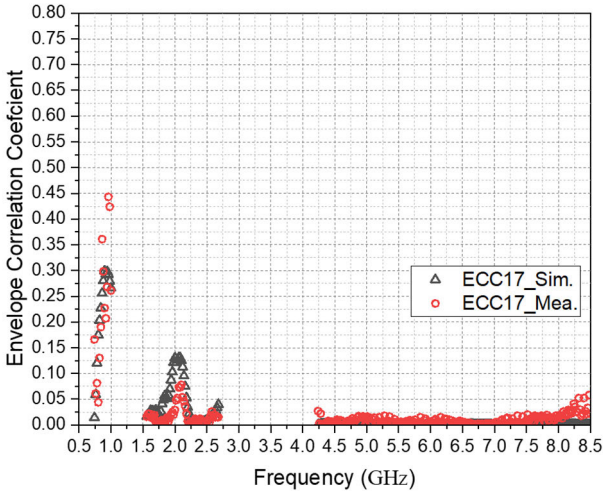

FIGURE 41. Comparison diagram of ECC simulation and actual measurement of Ant. 1 and Ant. 7.

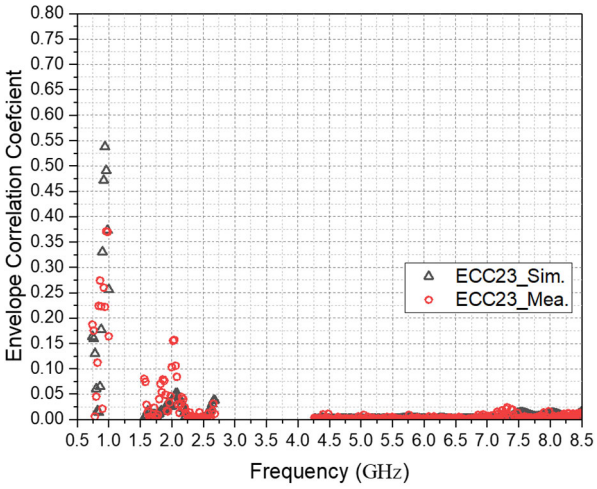

FIGURE 42. Comparison diagram of the ECC simulation and actual measurement of Ant. 2 and Ant. 3.

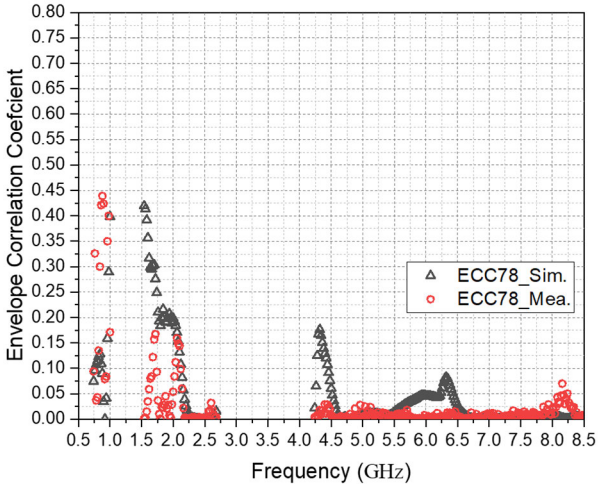

FIGURE 43. Comparison diagram of ECC simulation and actual measurement of Ant. 7 and Ant. 8.

within the chamber aligns with the XYZ axes of the chamber, as defined by the simulation software.

Figure 31 illustrates the 2D radiation patterns of Ant. 1 in the XY plane, XZ plane, and YZ plane for the 10 × 10 MIMO antenna system on the full metal backplane of a laptop computer. The simulation results are compared with the measurement results. It can be observed from the Figure 31 that at the resonant frequencies of 0.8 GHz, 0.94 GHz, 1.83 GHz, 2.32 GHz, 4.33 GHz, 5.66 GHz, and 6.74 GHz, the simulated and measured radiation patterns exhibit similar trends.

This indicates that the radiation characteristics of Ant. 1 at these resonant frequencies show good agreement between simulation and measurement. This consistency is crucial for antenna design and performance evaluation, and confirms that the 10 × 10 MIMO antenna system on the full metal backplate of the laptop computer exhibits reliable radiation patterns in the far-field direction.

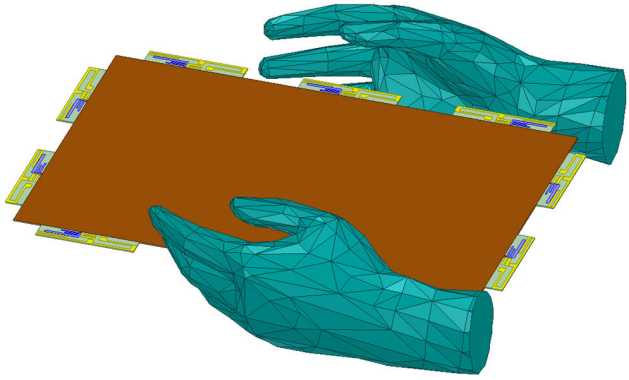

FIGURE 44. Schematic diagram of the configuration when the user holds it with both hands in the long-hand direction.

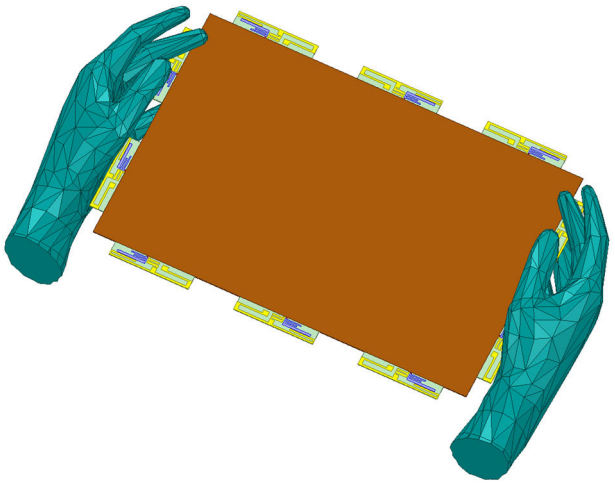

FIGURE 45. Schematic diagram of the configuration when the user holds it with both hands in the short side direction.

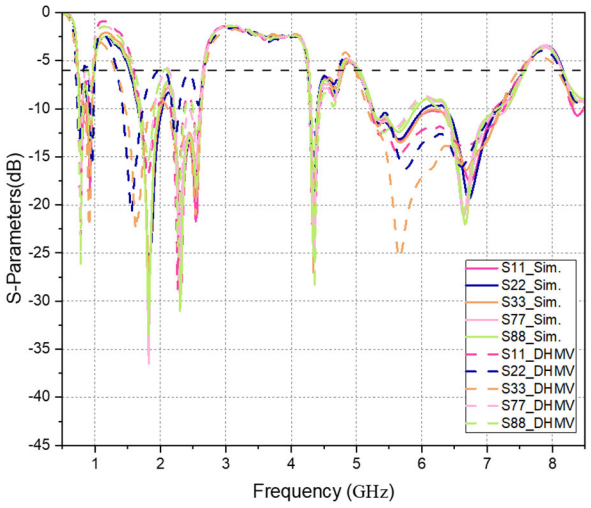

FIGURE 46. Comparative schematic of the reflection coefficients for Ant. 1-3, 7, and 8 between the antenna system shown in Figure 1 and the system depicted in Figure 45.

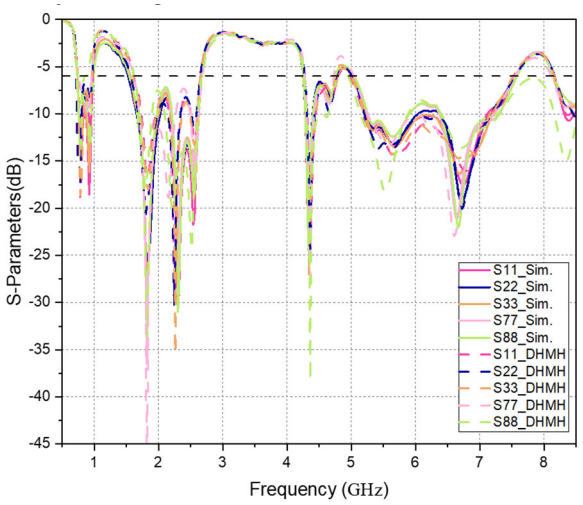

FIGURE 47. Comparative schematic of the reflection coefficients for Ant. 1-3, 7, and 8 between the antenna system as illustrated in Figure 1 and the system depicted in Figure 46.

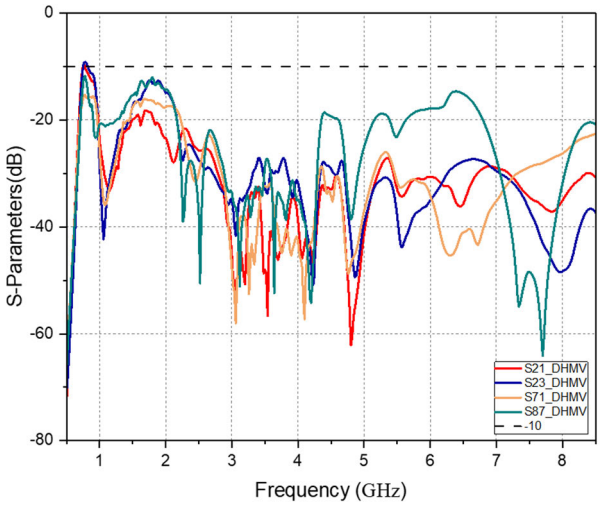

FIGURE 48. Comparative schematic of the penetration coefficients for Ant. 1-3, 7, and 8 between the antenna system shown in Figure 1 and the system depicted in Figure 45.

Figure 32 is a 2D radiation pattern diagram of the simulated and measured results of the Ant. 2 in the XY plane XZ plane and YZ plane of the all-metal backplane 10 × 10 MIMO antenna system of the notebook computer. It can be seen from the Figure 32 that when Ant. 1 operates at the resonance points of 0.8 GHz, 0.94 GHz, 1.83 GHz, 2.32 GHz, 4.33 GHz, 5.66 GHz and 6.74 GHz, the simulated and measured radiation modes have the same trend.

Figure. 33 is a 2D gain pattern diagram of the simulated and system on the XY plane XZ plane and YZ plane of the all- measured results of the Ant. 7 of the 10 × 10 MIMO antenna metal backplane of the notebook computer. It can be seen from the Figure 33 that when Ant. 1 operates at the resonance points of 0.8 GHz, 0.94 GHz, 1.83 GHz, 2.32 GHz, 4.33 GHz, 5.66 GHz and 6.74 GHz, the simulated and measured radiation modes have the same trend.

C. GAIN AND EFFICIENCY

In this paper, we further compare the gain and radiation efficiency of the antennas. In Figure 34, the simulated Ant. 1 shows peak gains of 2 dB, 4 dB, 2 dB, and 7 dB at frequencies of 0.8 GHz, 2.2 GHz, 4.5 GHz, and 7.4 GHz, respectively. The measured antenna gains are 4.7 dB at 0.8 GHz, 4 dB at 2.2 GHz, 2.59 dB at 4.5 GHz, and 3.65 dB at 7.4 GHz.

Additionally, in Figure 35, the simulated Ant. 1 exhibits radiation efficiencies of 69%, 77%, 43%, and 73% at frequencies of 0.8 GHz, 2.2 GHz, 4.5 GHz, and 7.4 GHz, respectively. On the other hand, the measured radiation efficiencies are 82% at 0.8 GHz, 86% at 2.2 GHz, 63% at 4.5 GHz, and 60% at 7.4 GHz.

In Figure 36, the simulated Ant. 2 exhibits peak gains of 2.4 dB, 3 dB, 0.07 dB, and 7.1 dB at frequencies of 0.8 GHz,

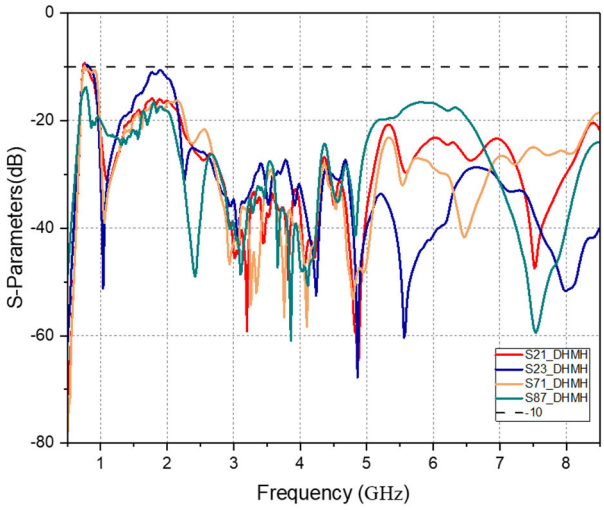

FIGURE 49. Comparative schematic of the penetration coefficients for Ant. 1-3, 7, and 8 within the antenna system shown in Figure 1 and the system shown in Figure 46.

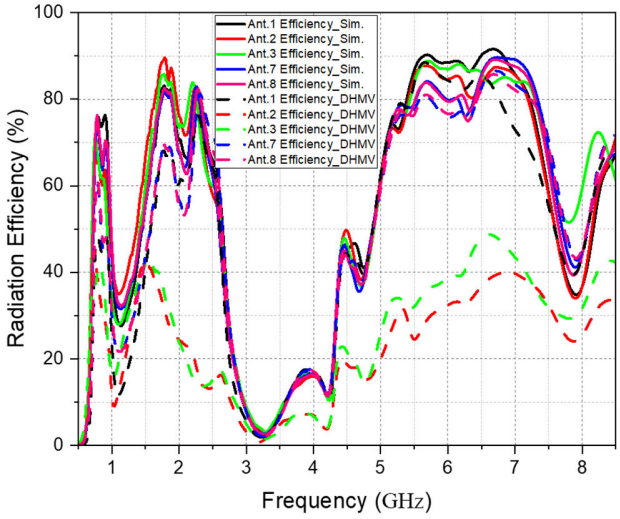

FIGURE 50. Comparative schematic of efficiency for Ant. 1-3, 7, and 8 between the antenna system shown in Figure 1 and the system depicted in Figure 45.

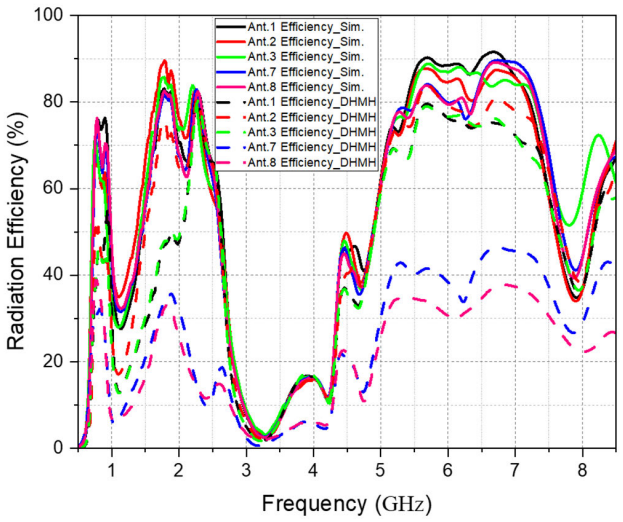

FIGURE 51. Comparative schematic illustrating the efficiency of Ant. 1-3, 7, and 8 in the antenna system shown in Figure 1 compared to the system depicted in Figure 46.

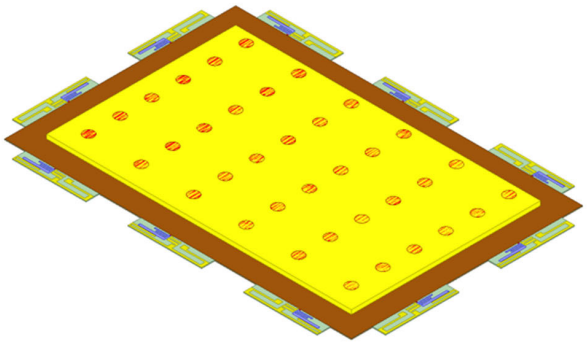

FIGURE 52. Schematic diagram showing the placement of a battery on the antenna system as illustrated in Figure 1.

2.2 GHz, 4.4 GHz, and 7.4 GHz, respectively. The measured antenna gains are 5.3 dB at 0.8 GHz, 3.17 dB at 2.2 GHz, 1.09 dB at 4.5 GHz, and 3.7 dB at 7.4 GHz.

Similarly, in Figure 37, the simulated Ant. 2 shows peak radiation efficiencies of 64%, 78%, 43%, and 73% at frequencies of 0.8 GHz, 2.2 GHz, 4.5 GHz, and 7.4 GHz, respectively. The measured radiation efficiencies are 96% at 0.8 GHz, 84% at 2.2 GHz, 59% at 4.4 GHz, and 59% at7.4 GHz.

In Figure 38, the simulated Ant. 7 shows gains of 1.45 dB, 3.3 dB, 4.15 dB, and 5.2 dB at frequencies of 0.8 GHz, 2.2 GHz, 4.5 GHz, and 7.4 GHz, respectively. The measured antenna gains are 1.6 dB at 0.8 GHz, 5.6 dB at 2.2 GHz, 4.4 dB at 4.5 GHz, and 3.65 dB at 7.4 GHz.

Similarly, in Figure 39, the simulated Ant. 7 exhibits peak radiation efficiencies of 80%, 76%, 45%, and 75% at frequencies of 0.8 GHz, 2.2 GHz, 4.5 GHz, and 7.4 GHz, respectively. The measured radiation efficiencies are 57% at 0.8 GHz, 86% at 2.2 GHz, 53% at 4.5 GHz, and 64% at7.4 GHz.

IV. ENVELOP CORRELATION COEFFICIENT (ECC)

The Envelope Correlation Coefficient (ECC) is a crucial metric for assessing the performance of MIMO antenna systems.

The formula for calculating ECC is related to the S-parameters, and it is as follows: [24]

$$ECC_{ij} = \frac{\left|S_{ii}^{*}S_{ij} + S_{ji}^{*}S_{jj}\right|^{2}}{\left(1 - \left(\left|S_{ij}\right|^{2} + \left|S_{ji}\right|^{2}\right)\right)\left(1 - \left(\left|S_{jj}\right|^{2} + \left|S_{ij}\right|^{2}\right)\right)}$$

where i and j are antennas at different locations.

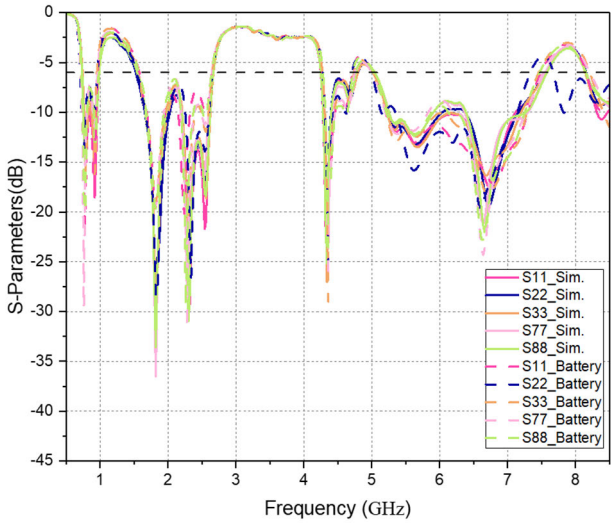

FIGURE 53. Comparative schematic of the reflection coefficients for the antenna system shown in Figure 1 and with the battery setup as depicted in Figure 53.

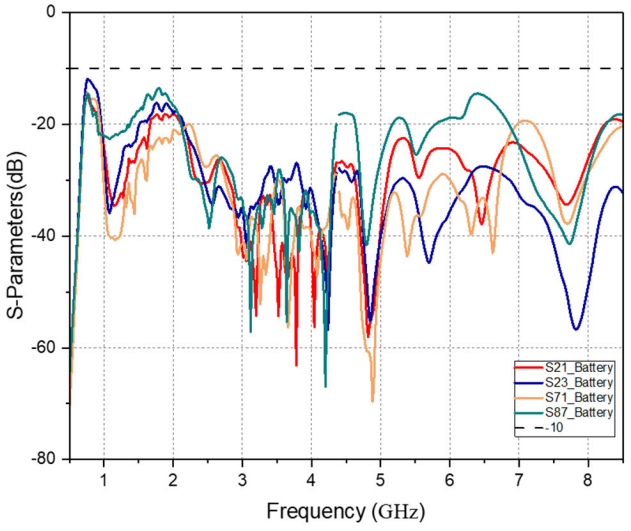

FIGURE 54. Comparative schematic of the penetration coefficients for the antenna system shown in Figure 1 and with the battery setup as depicted in Figure 53.

Figures 40 to 43 present the simulated and measured ECC results for the antenna pairs in the 10 × 10 MIMO antenna system on the full-metal backplane of the laptop.

Specifically, the ECC values are shown for Ant. 1 and Ant. 2, Ant. 2 and Ant. 3, Ant. 1 and Ant. 7, as well as Ant. 7 and Ant. 8.

Within the effective operating frequency range, both the measured and simulated ECC values remain below 0.5 for all antenna pairs. This observation indicates that Ant. 1 and Ant. 2, Ant. 2 and Ant. 3, Ant. 1 and Ant. 7, as well as Ant. 7 and Ant. 8, exhibit good isolation and independence from each other frequencies of 0.8 GHz, 2.2 GHz, 4.5 GHz, and 7.4 GHz, respectively. The measured radiation efficiencies are 57% at 0.8 GHz, 86% at 2.2 GHz, 53% at 4.5 GHz, and 64% at7.4 GHz.

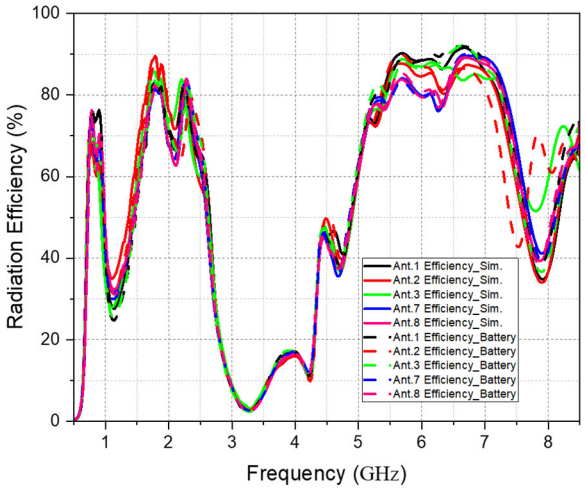

FIGURE 55. Comparative schematic of the efficiency for Ant. 1-3, 7, and 8 in the antenna system shown in Figure 1 and the system with a battery as depicted in Figure 53.

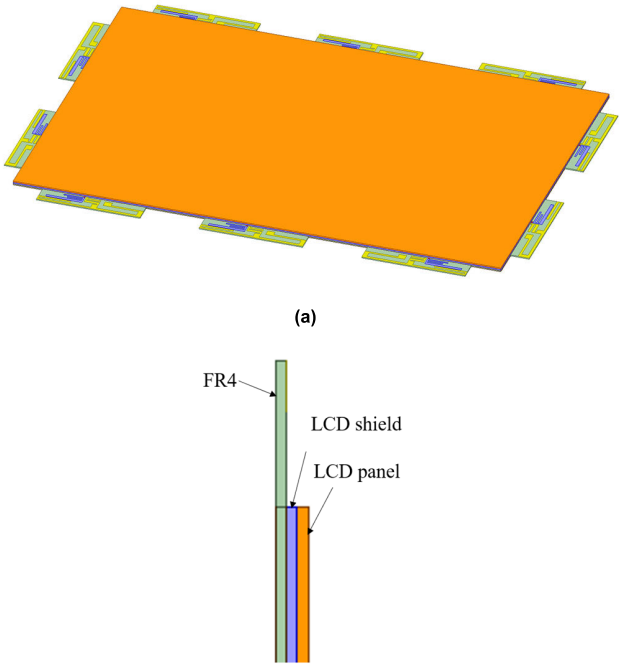

FIGURE 56. (a) A three-dimensional schematic showing the placement of an LCD module on the antenna system as illustrated in Figure 1. (b) An enlarged side view schematic of Figure 57(a).

V. IMPACT OF EXTERNAL FACTORS ON ANTENNA PERFORMANCE

A. EFFECT OF USER HAND

In this section, the impact of the user's hands on the antenna system is examined when the device is held in different orientations, as illustrated in Figure 1. Figure 44 shows the configuration when the user holds the device along its longer edge, causing Ant. 2, 3, 5, and 6 to be obscured by the hands, while Ant. 1, 4, 7, 8, 9, and 10 remain unobscured. Figure 45 shows the setup for when the device is held along

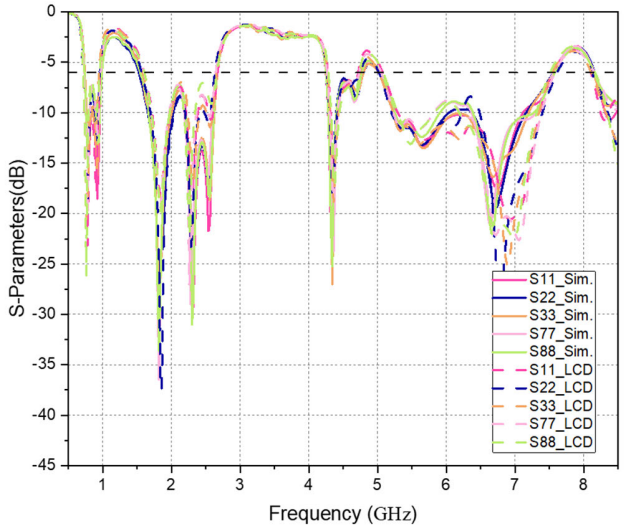

FIGURE 57. Comparative schematic of the reflection coefficients for the antenna system shown in Figure 1 and with the setup of the LCD module as shown in Figure 57.

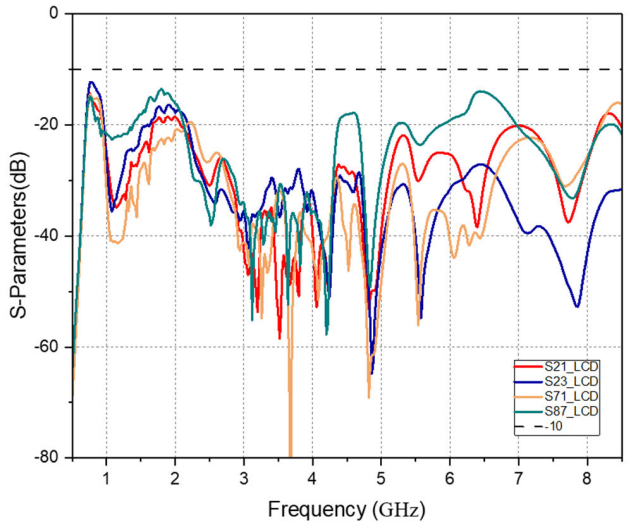

FIGURE 58. Comparative schematic of the penetration coefficients for the antenna system shown in Figure 1 and with the LCD module setup as depicted in Figure 57.

its shorter edge, with the user's hands obscuring Ant. 7 to 10, leaving Ant. 1 to 6 unobscured. This analysis highlights the significant effect of hand placement on the performance and functionality of the antenna system in practical usage scenarios.

Figure 46 illustrates the comparison of reflection coefficients for Ant. 1-3, 7, and 8 in the unobstructed antenna system shown in Figure 1 and the system with hands covering Ant. 2, 3, 5, and 6 as shown in Figure 44. Similarly, Figure 47 shows this comparison for the system in

Figure 1 and the system with hands that obscure Ant. 7-10, as shown in Figure 45. Due to the symmetrical design of the antenna system, the discussion will focus on Ant. 1-3, 7, and 8. It is observed that regardless of the orientation in which hands are obscured, the impact on the reflection coefficient is remarkably low.

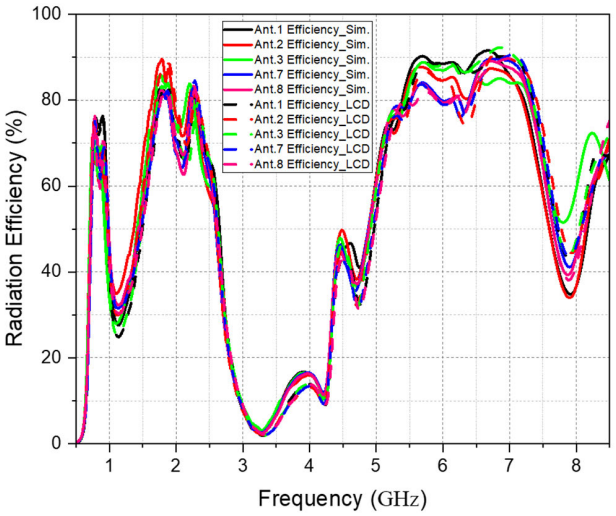

FIGURE 59. Comparative schematic illustrating the efficiency of Ant. 1-3, 7, and 8 in the antenna system shown in Figure 1 and the system with an LCD module as shown in Figure 57.

Figure 48 presents a comparison of the penetration coefficients for Ant. 1-3, 7, and 8 between the antenna system shown in Figure 1 and the system depicted in Figure 44. Similarly, Figure 49 compares these coefficients for the system in Figure 1 and the system shown in Figure 45. It is observed that regardless of the direction from which the user holds the antenna system as introduced in Figure 1, the penetration coefficient between the antenna systems remains better than 10dB.

Due to hand obstruction over Ant. 2, 3, 5, and 6 in the antenna system depicted in Figure 44, the efficiency of Ant. 2 and 3 significantly decreases as illustrated in Figure 50, while Ant. 1, 7, and 8, not being obscured, are almost unaffected. Similarly, in the antenna system shown in Figure 45 where hands obscure Ant. 7 and 8, the efficiency of Ant. 7 and 8 is notably reduced as shown in Figure 51, whereas Ant. 1-3, not being obscured, remain almost unaffected.

B. EFFECT OF BATTERY

In this section, as illustrated in Figure 52, a metal block with dimensions of 180 × 290 × 4mm is assumed to be equivalent to the battery of a laptop and is placed on the antenna system shown in Figure 1. Additionally, 36 shorting pins are positioned between the metal block and the ground plane.

Figure 53 compares the reflection coefficients of the antenna system before and after the addition of a battery, as shown in Figure 52. It demonstrates that even with the inclusion of a battery in the proposed antenna system, the impact on the reflection coefficient remains significantly low.

As shown in Figure 54, adding a battery to the antenna system proposed in Figure 1 results in the system's penetration coefficient remaining above 10dB. This indicates that the inclusion of a battery does not significantly hinder the

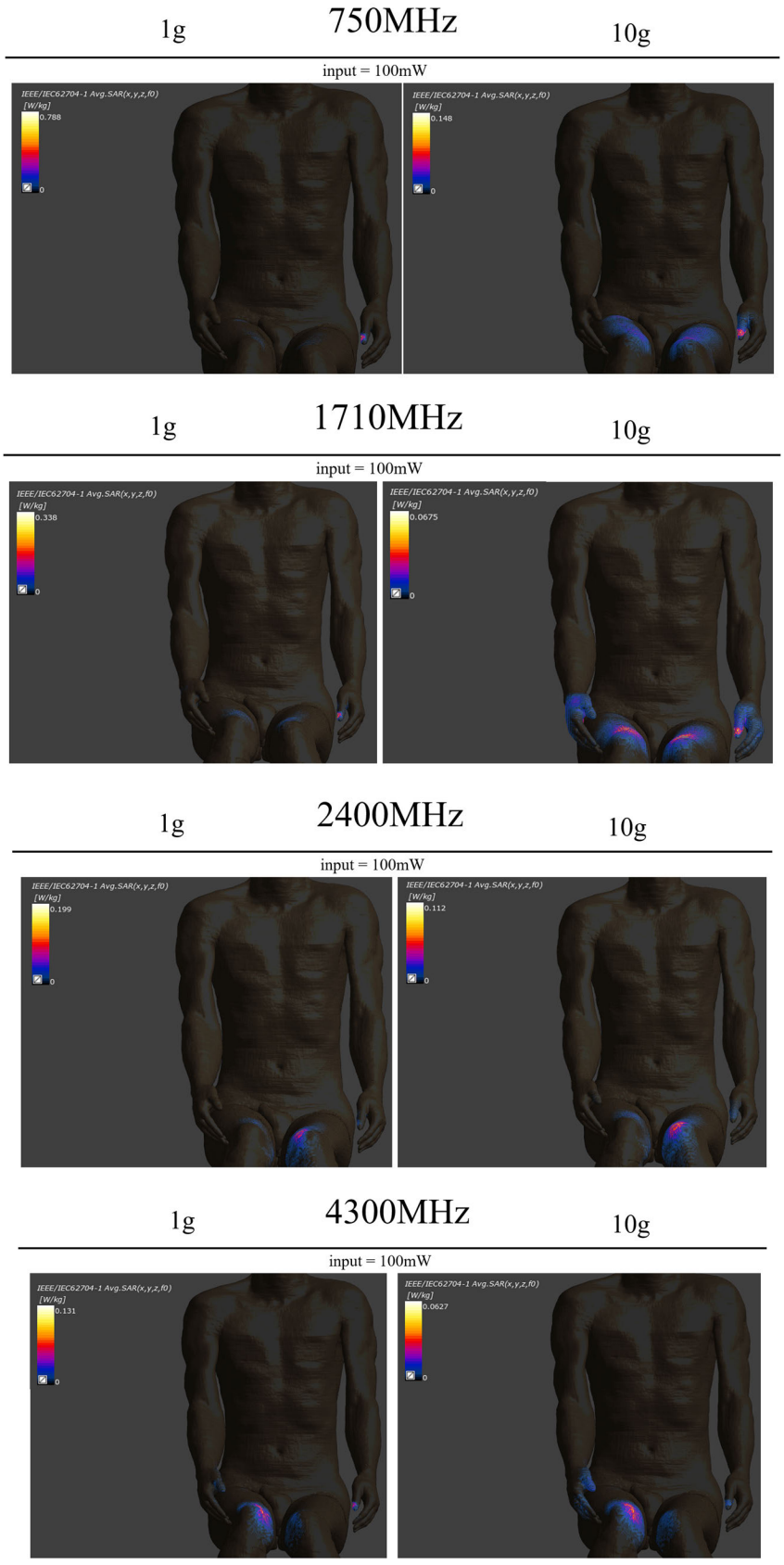

FIGURE 60. SAR simulation results of Ant. 1 at 0.75 GHz, 1.71 GHz, 2.4 GHz, 4.3 GHz, 5.85 GHz.

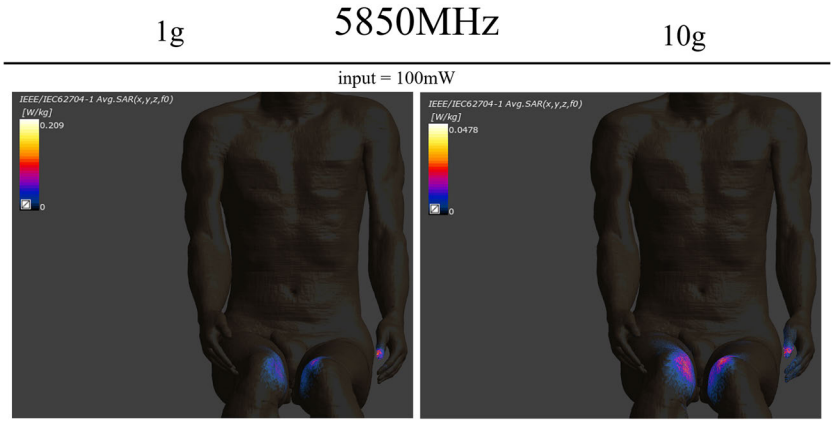

FIGURE 60. *(Continued.)* **SAR simulation results of Ant. 1 at 0.75 GHz, 1.71 GHz, 2.4 GHz, 4.3 GHz, 5.85 GHz.**

TABLE 2. **SAR of Antenna 1.**

Frequency(GHz)	1gSAR(W/kg)	10gSARW/kg
0.8	0.788	0.148
0.94	0.338	0.0675
1.83	0.199	0.112
2.32	0.131	0.0627
4.33	0.209	0.0478
5.64	0.788	0.148
6.74	0.338	0.0675

system's ability to maintain effective signal transmission, highlighting the robustness of the antenna design.

As shown in Figure 55, the efficiency of Ant. 1-3, 7, and 8 within the antenna system remains almost unaffected even after the integration of a battery. This demonstrates the system's robust performance in terms of antenna efficiency, ensuring that modifications such as the addition of a battery do not compromise its signal transmission and reception quality.

C. EFFECT OF THE LCD MODULE

In this section, as depicted in Figure 56, it is assumed that a stainless steel block measuring 330 × 220 × 1mm serves as the LCD shield, and a glass piece of the same dimensions acts as the LCD Panel. The LCD shield is positioned on the ground plane of the antenna system, with the LCD Panel placed on top of the LCD shield.

From Figure 57, a comparison of the reflection coefficients between the antenna system shown in Figure 1 and the system with an LCD module is presented as depicted in Figure 57. It is observed that the inclusion of an LCD module in the proposed antenna system has a minimal impact on the reflection coefficient, indicating that the system's design effectively accommodates the integration of additional components without significantly affecting its performance.

Figure 58 shows a comparison of the penetration coefficients for Ant. 1-3, 7, and 8 between the antenna system shown in Figure 1 and the system with an LCD module as shown in Figure 57. After adding the LCD module to the antenna system proposed in Figure 1, the penetration coefficient between the antenna systems still remains better than 10dB.

As indicated in Figure 59, the efficiency of Ant. 1-3, 7, and 8 within the antenna system remains nearly unaffected even after the addition of an LCD module. This highlights the system's robust design in maintaining antenna performance despite the integration of additional components.

VI. HUMAN BODY EFFECT ANALYSIS (SAR)

Electronic products that are in close proximity to the human body use antennas for wireless communication, and during this transmission, electromagnetic radiation is generated. Therefore, it is important to assess the Specific Absorption Rate (SAR) values and perform simulations to ensure compliance with regulatory guidelines.

In this study, the proposed antenna system is symmetric or mirror-symmetric in its configuration. Therefore, SAR simulations are conducted only for Ant. 1. The SAR at a distance from the thigh, and an input power of 100 mW (20dBm) is applied at frequencies of 0.75 GHz, 1.71 GHz, 2.4 GHz, 4.3 GHz, and 5.85 GHz simulations are performed using the software Sim4Life, as shown in Figure 60. Ant. 1 is placed 0.75 GHz, 1.71GHz, 2.4 GHz, 4.3GHz, and 5.85 GHz to calculate the 1g and 10g SAR values.

The simulation results indicate that the SAR values for Ant. 1 at 0.75GHz, 1.71 GHz, 2.4 GHz, 4.3GHz, and 5.85 GHz are well below the regulatory limits, as shown in Table 2. This confirms that the proposed antenna system complies with SAR regulations.

VII. COMPARISON WITH OTHER ANTENNAS

Table 3 provides a comparison between the proposed Ant. 1 in this study and other existing antenna research. From

TABLE 3. Antenna comparison table.

Ref.	Size(mm)	Apply to	Operating Band (GHz)	Eff.(%)	Gain (dBi)	MIMO	Isolation (dB)	ECC
[2]	130 × 3	Laptop	LTE700/GSM850/900/1800/1900/UMTS/LTE2300/2500	40-50	0.5~1.9	2×2	>16	<0.2
[5]	5 × 12	Phone	3.3-3.8	87-93	5.3	18	>20	<0.01
[8]	9.5 × 3	Phone	3.4–3.8 5.15–5.925	>42 >62	N/A	10	11	0.15 0.05
[9]	15 × 3	Laptop	3.4-3.8 4.8-5	≥ 42	N/A	4	>10	≤0.27
[12]	0.35λ × 0.13 λ	Laptop	2.3 2.4 3.3 5	82.9 81.6 84.2	4.9 5.6 4.25	N/A	N/A	N/A
[14]	60 × 10 × 0.8	Laptop	LTE 2300/2500/WLAN 2.4 GHz/ 5G C-band	53.6-70.3 56.7-66.7	2.9~4.9	3	N/A	≤0.15
[16]	17.5×4	Laptop	5.1-5.92	83.50-89.20	4.45-5.22	N/A	N/A	N/A
[17]	50 ×5	Laptop	LET700/GSM850/900/GSM1800/1900/UMTS/LTE2300/2500	≥40	N/A	2×2	≥24	N/A
[20]	0.03λ × 0.22λ × 0.02λ	Phone	3.4–3.8 5.15–5.925	83-93	5.3	10×10	>20	<0.06
[21]	32×2	Laptop	3.3-3.6 4.8-5	≥40	N/A	8×8	>10	
This work	70×12.5 (0.17λ× 0.03λ× 0.00197λ)	Laptop (Tablet) (Phone)	0.74-0.99 1.38-2.64 4.3-4.7 4.8-6.58	≥43	4.7 4 2.59 3.65	10×10	>10	0.5

the Table 3, it can be observed that the dimensions of Ant. 1 in this study are similar to the antennas with frequencies below 1 GHz found in the literature. Antennas with smaller dimensions in the literature do not cover frequencies below 1 GHz. Furthermore, Ant. 1 in this study covers more frequency bands compared to the entire literature, and it has the highest number of antennas in the MIMO system.

The gain and efficiency of Ant. 1 in this study also do not differ significantly from the literature, with the isolation level being at least −10 dB and the ECC being less than 0.5 for all frequency bands.

VIII. CONCLUSION

Based on the comprehensive comparison, the proposed antenna in this study covers a broader range of frequency bands and has a larger number of antennas, with consistent reflection coefficients across different positions. This indicates that the antenna design in this study exhibits robustness and is well suited for applications on notebook computers. Furthermore, the design could be extended to be applied in tablet computers and smartphones. The dimensions of the proposed antenna are already comparable to antennas with frequencies below 1 GHz in the literature, leaving room for potential further size reduction by incorporating passive components into the antenna design.

REFERENCES

[1] S.-C. Chen, J.-Y. Nieh, W.-H. Liao, and S.-M. Li, "DTV/LTE antennas with no physical structure for laptop computers," *J. Electromagn. Waves Appl.*, vol. 35, no. 11, pp. 1448–1463, Jul. 2021.

[2] S.-C. Chen and M.-C. Hsu, "LTE MIMO closed slot antenna system for laptops with a metal cover," *IEEE Access*, vol. 7, pp. 28973–28981, 2019.

[3] Y. Fang, Y. Liu, Y. Jia, J. Liang, and H. H. Zhang, "Reconfigurable structure reutilization low-SAR MIMO antenna for 4G/5G full-screen metal-frame smartphone operation," *IEEE Antennas Wireless Propag. Lett.*, vol. 22, no. 5, pp. 1219–1223, 2023.

[4] Y. Wang and F. Xu, "Shared-aperture 4G LTE and 5G mm-wave antenna in mobile phones with enhanced mm-wave radiation in the display direction," *IEEE Trans. Antennas Propag.*, vol. 71, no. 6, pp. 4772–4782, 2023.

[5] N. Jaglan, S. D. Gupta, and M. S. Sharawi, "18 element massive MIMO/Diversity 5G smartphones antenna design for sub-6 GHz LTE bands 42/43 applications," *IEEE Open J. Antennas Propag.*, vol. 2, pp. 533–545, 2021.

[6] X.-H. Ding, Q.-H. Zhang, W.-W. Yang, W. Qin, L. Guo, and J.-X. Chen, "A dual-band antenna for LTE/mmWave mobile terminal applications," *IEEE Trans. Antennas Propag.*, vol. 71, no. 3, pp. 2826–2831, Mar. 2023.

[7] R. Ullah, S. Ullah, R. Ullah, F. Faisal, I. B. Mabrouk, and M. J. A. Hasan, "A 10-ports MIMO antenna system for 5G smart-phone applications," *IEEE Access*, vol. 8, pp. 218477–218488, 2020.

[8] V. Thakur, N. Jaglan, and S. D. Gupta, "Side edge printed eight-element compact MIMO antenna array for 5G smartphone applications," *J. Electromagn. Waves Appl.*, vol. 36, no. 12, pp. 1685–1701, Aug. 2022.

[9] S.-C. Chen, J.-L. Zhu, and Chung-I. G. Hsu, "Compact double shorted loop sub-6-GHz dual-band MIMO quad-antenna system," *IEEE Access*, vol. 9, pp. 114672–114679, 2021.

[10] S. Padmanathan, A. A. Al-Hadi, A. M. Elshirkasi, S. S. Al-Bawri, M. T. Islam, T. Sabapathy, M. Jusoh, P. Akkaraekthalin, and P. J. Soh, "Compact multiband reconfigurable MIMO antenna for sub- 6GHz 5G mobile terminal," *IEEE Access*, vol. 10, pp. 60241–60252, 2022.

[11] J. S. Kulkarni, "An ultra-thin, dual band, sub 6 GHz, 5G and WLAN antenna for next generation laptop computers," *Circuit World*, vol. 46, no. 4, pp. 363–370, Apr. 2020.
[12] J. Kulkarni, "Multiband triple folding monopole antenna for wireless applications in the laptop computers," *Int. J. Commun. Syst.*, vol. 34, no. 8, p. e4776, May 2021.
[13] A. M. Elshirkasi, A. A. Al-Hadi, R. Khan, P. Akkaraekthalin, H. S. B. Abdelmula, A. M. Belghasem, A. H. Jebril, and P. J. Soh, "Numerical analysis of users' body effects on a fourteen-element dual-band 5G MIMO mobile terminal antenna," *IEEE Access*, vol. 10, pp. 2083–2096, 2022.
[14] W. Chen and R. Lin, "Three-port MIMO antennas for laptop computers using an isolation element as a radiator," *Int. J. RF Microw. Comput.-Aided Eng.*, vol. 31, no. 2, p. e22326, Feb. 2021.
[15] S.-C. Chen, W.-S. Cai, C.-I.-G. Hsu, and L.-C. Chou, "Low-profile WLAN MIMO PIFA antenna system for laptops with large screen," *IETE J. Res.*, vol. 68, no. 2, pp. 990–998, Mar. 2022.
[16] J. Kulkarni, N. Kulkarni, and A. Desai, "Development of 'H-shaped' monopole antenna for IEEE 802.11 a HIPERLAN 2 applications in the laptop computer," *Int. J. RF Microw. Comput.-Aided Eng.*, vol. 30, no. 7, 2020, Art. no. e22233.
[17] S.-C. Chen and K.-Y. Li, "Integrated planar LTE MIMO dual-antenna system on laptop computer's hinge," *IETE J. Res.*, vol. 69, no. 4, pp. 1881–1890, 2021.
[18] S.-C. Chen, P.-W. Wu, C. G. Hsu, and J.-Y. Sze, "Integrated MIMO slot antenna on laptop computer for eight-band LTE/WWAN operation," *IEEE Trans. Antennas Propag.*, vol. 66, no. 1, pp. 105–114, Jan. 2018.
[19] J. Kulkarni and C. Sim, "Multiband, miniaturized, maze shaped antenna with an air-gap for wireless applications," *Int. J. RF Microw. Comput.-Aided Eng.*, vol. 31, no. 1, Jan. 2021, Art. no. e22502.
[20] N. Jaglan, S. D. Gupta, B. K. Kanaujia, and M. S. Sharawi, "10 element sub-6-GHz multi-band double-T based MIMO antenna system for 5G smartphones," *IEEE Access*, vol. 9, pp. 118662–118672, 2021.
[21] S. Chen, J. Zhu, and C. G. Hsu, "Compact closed-slot eight-antenna system for 5G laptops with a metal back cover," *Int. J. Commun. Syst.*, vol. 34, no. 18, p. e4986, Dec. 2021.
[22] C. Lee and S. Su, "Decoupled multi-input multi-output antennas with a common dipole for wideband 5G laptop computers," *Microw. Opt. Technol. Lett.*, vol. 63, no. 4, pp. 1286–1293, Apr. 2021.
[23] H. Aliakbari, L. Y. Nie, and B. K. Lau, "Large screen enabled tri-port MIMO handset antenna for low LTE bands," *IEEE Open J. Antennas Propag.*, vol. 2, pp. 911–920, 2021.
[24] H. Wang, R. Zhang, Y. Luo, and G. Yang, "Compact eight-element antenna array for triple-band MIMO operation in 5G mobile terminals," *IEEE Access*, vol. 8, pp. 19433–19449, 2020.

MING-AN CHUNG (Senior Member, IEEE) received the B.Eng. and M.Eng. degrees in electronic engineering from Chang Gung University, Taoyuan, Taiwan, in 2003 and 2005, respectively, and the D.Eng. degree in electrical engineering from the National Taiwan University of Science and Technology (NTUST), Taipei, Taiwan, in 2016. He is currently an Associate Professor with the Department of Electronic Engineering, National Taipei University of Technology (NTUT), where he is also the Leader of the Innovation Wireless Communication and Electromagnetic Applications Laboratory. His research interests include wireless communication propagation, intelligent robotics, self-driving vehicles, antenna design for various mobile and wireless communications, electromagnetic theory, and applications. He is also a Reviewer of many scientific journals, including IEEE TRANSACTIONS ON ANTENNAS AND PROPAGATION, IEEE TRANSACTIONS ON INDUSTRIAL INFORMATICS, *Journal of Intelligent & Robotic Systems*, *IET Microwaves, Antennas and Propagation*, IEEE ANTENNAS AND WIRELESS PROPAGATION LETTERS, *International Review of Electrical Engineering*, *International Journal on Communications Antenna and Propagation*, and *AEÜ - International Journal of Electronics and Communications*, and many international conferences, including ICRA, ICCE-TW, RFIT, ICBEB, EMCAR, and SNSP.

MING-CHANG LEE received the B.S. degree from Taipei University of Marine Technology, in 2009, and the M.S. degree from National Taipei University of Technology, in 2023. His research interests include composite material antenna design, switched-beam antenna systems, MIMO antenna systems, millimeter wave antenna design, and phased array antenna.

CHIA-CHUN HSU received the Associate degree in computer and communication engineering from Army Academy R.O.C., Taiwan, in 2015. Her current research interests include antennas, MIMO antenna system design, the AIoT, and emotion recognition applications.

CHIA-WEI LIN received the B.S. and M.S. degrees from Chung Yuan Christian University, in 2007. He is currently pursuing the Ph.D. degree in electrical engineering with the National Taipei University of Technology. His research interests include wireless communication propagation research, antenna design, intelligent robotics research, self-driving vehicle research, embedded systems, and deep learning.